Accepted Manuscript

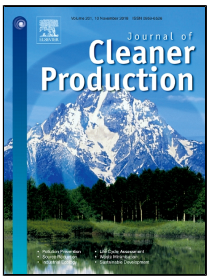

Experimental and numerical study of flexural behavior of novel oil palm concrete filled steel tube exposed to elevated temperature

Muhammad Faisal Javed, Nor Hafizah Binti Ramli Sulong, Shazim Ali Memon, Sardar Kashif-ur-Rehman, Niaz Bahadur Khan

PII:	S0959-6526(18)32744-6
DOI:	10.1016/j.jclepro.2018.09.032
Reference:	JCLP 14167
To appear in:	*Journal of Cleaner Production*
Received Date:	03 June 2018
Accepted Date:	04 September 2018

Please cite this article as: Muhammad Faisal Javed, Nor Hafizah Binti Ramli Sulong, Shazim Ali Memon, Sardar Kashif-ur-Rehman, Niaz Bahadur Khan, Experimental and numerical study of flexural behavior of novel oil palm concrete filled steel tube exposed to elevated temperature, *Journal of Cleaner Production* (2018), doi: 10.1016/j.jclepro.2018.09.032

Title: Experimental and numerical study of flexural behavior of novel oil palm concrete filled steel tube exposed to elevated temperature

Muhammad Faisal Javed
Address: Department of Civil Engineering, Sarhad University of Information & Technology, Peshawar, Pakistan
Email: arbabf1@gmail.com,

2. Dr. Nor Hafizah Binti Ramli @ Sulong
Address: Department of Civil Engineering, Faculty of Engineering, University of Malaya, 50603 Kuala Lumpur, Malaysia
Email: hafizah_ramli@um.edu.my

3. Dr. Shazim Ali Memon
Address: Department of Civil Engineering, School of Engineering, Nazarbayev University, Astana, Republic of Kazakhstan **Email:** shazimalimemon@gmail.com

4. Sardar Kashif-ur-Rehman
Address: Department of Civil Engineering, City University of Science & Information Technology, Pakistan
Email: kashif@engineersdaily.com

5. Niaz Bahadur Khan
Address: School of Mechanical and Manufacturing Engineering, National University of Sciences and Technology, Islamabad, Pakistan
Email: n_bkhan@yahoo.com

Experimental and numerical study of flexural behavior of novel oil palm concrete filled steel tube exposed to elevated temperature

Abstract

Oil palm boiler clinker (OPB) is a waste byproduct obtained at elevated temperature in an oil palm processing mill. Moreover, in recent years, Concrete filled steel tube (CFST) has been used widely in structures throughout the world. This paper presents an experimental and numerical study on novel sustainable composite beam by using OPB as replacement of natural coarse aggregate in CFSTs. Steel hollow beams (3.2m length) infilled with natural aggregate concrete and OPB concrete were subjected to flexural load and elevated temperature. The parameters selected for the experimental tests were the cross-section type (square, rectangular) and the infilling type (natural aggregate concrete and OPB concrete). The thermal response, failure modes, critical temperature, temperature distribution in steel tube and infilled concrete, deflection along the span and fire concrete contribution ratio were evaluated. The critical temperature and fire concrete contribution ratio of OPB CFST was found to be higher than natural aggregate CFST, showing superior performance of OPB CFST. Thereafter, simulations were performed and more than 50 models were analyzed to evaluate the effect of yield strength of steel (235-400 MPa), compressive strength of infilled concrete (30-75 MPa), load ratio (0.3-0.6), width-to-depth ratio (2-0.5) and steel ratio (4.4%-2.1%) on the fire resistance time of CFST beam. It was found that the increase in load ratio, steel ratio and yield strength of steel has adverse effected on the fire resistance (FR) time of CFST member. However, the FR time increased significantly with an increase in compressive strength of infilled concrete and cross-sectional dimension of CFST member. Finally, the experimental results were compared with existing equations for CFST columns filled with natural aggregate concrete. It was found that current equations may underestimate the fire resistance of CFST filled with OPB.

1. Introduction

Malaysia palm oil industry is the world's 2nd largest palm oil industry, with an annual production of 19.67 million metric tons of crude palm oil (Ibrahim et al., 2017). Despite producing valuable products, the palm oil industry also generates agricultural wastes (biomass). From the consumption of large amount of natural resources (forest land and water) (Javed et al., 2018; Musikavong and Gheewala, 2017a, b; Suttayakul et al., 2016) during cultivation, to the production of huge amount of environmental pollutants during processing, palm oil industry is severe threat to the environment. The pollutant produced from oil palm industry contributes to global warming, eutrophication, acidification and air pollution (Bessou et al., 2014; Saswattecha et al., 2015). That's why, oil palm industry is well known in many countries for its harmful environmental impacts. In Malaysia, 80 million dry solid biomass waste was yielded in 2010 only and is expected to reach up to 110 million by 2020 from palm oil industry only (Malaysia, 2011; Ng et al., 2012). Various types of solid wastes like palm fiber, oil palm shell, oil palm boiler clinker and empty fruit

branches are produced at the end of palm oil processing stages. Oil-palm-boiler clinker (OPB) is a waste material obtained by burning off solid wastes at elevated temperature of 850°C during the process of palm oil extraction (Aslam et al., 2016b; Jumaat et al., 2015). OPB usually has no economic value and are abundantly available (Hartono et al., 2016; Shafigh et al., 2014). Most of the OPB is used for covering the potholes on the roads within the vicinity of the plantation areas, which affect the environment directly (Kanadasan and Abdul Razak, 2015).

The construction industry in Malaysia is developing very rapidly and progressively to support the country's economy (Karim et al., 2018; Rehman et al., 2017). By utilizing the agricultural waste in the construction industry will be a smart choice as it will reduce the harm caused by agricultural and construction industries to the environment. Besides, sustaining green environment by utilizing the waste materials, OPB has lower density and can be used in the construction industry to produce lightweight concrete. Full aggregate substitution with OPB has been shown to reduce 30% of manufacturing cost and 22.62% reduction in carbon dioxide emission, with comparable structural efficiency (strength-to-weight ratio) to conventional mix concrete (Kanadasan and Razak, 2015). Hence, using the OPB as coarse aggregate in concrete instead of natural aggregate would be efficacious in terms of cost and sustainability of a structure. Moreover, for the same aggregate/cement and water/binder ratio, the OPB concrete has shown less compressive strength, modulus of elasticity and tensile strength by 30%, 20-25% and 16-32%, respectively when compared to conventional concrete (Aslam et al., 2016a, b). However, the durability and long term performance of OPB concrete is similar to conventional concrete (Mo et al., 2016; Rehman et al., 2016; Teo et al., 2007).

Concrete filled steel tubes combine the action of steel and concrete when resisting axial forces and bending moments, thus showing a superior structural performance. While the steel tube confines the infilled concrete thereby improving its compressive strength, the later extends the local buckling of steel tube. The confinement of concrete by the outer tube depends on the type of infilled concrete, size of member, yield strength of steel and type of material used as outer steel tube (Dong et al., 2015; Kashif Ur Rehman et al., 2018; Kwan et al., 2015; Wang et al., 2016). It is known that the fire resistance (FR) of CFST members is better than that of hollow steel tubular columns (Liu et al., 2018; Ukanwa et al., 2018; Ukanwa et al., 2017; Yu et al., 2018). In fact most of the times, the external protection is not needed for residential buildings, where CFST members are used (Romero et al., 2011; Wang, 2014). Wang and Kodur suggested to use CFST columns in order to reduce the cost of fire protection (Wang and Kodur, 2000). Hence, the use of CFST members has increased and became popular over the last years. The use of concrete made with other than natural/normal aggregates (waste aggregates, recycled aggregates, lightweight aggregates) as infilling in CFST members is very popular amongst designers and has recently became a good alternative to Natural Aggregate Concrete (NAC) (Fu et al., 2015; Li et al., 2017; Silva et al., 2016). Among such types, the lightweight waste aggregate concrete has attracted a considerable attention due to its higher strength to weight ratio compared to the NAC. In addition, the high demand of NAC has significantly reduced the natural stone deposits and caused an

immense damage to the environment. At room temperature, OPB CFST (OCFST) columns show higher load-bearing capacity than traditional NAC filled steel tube (NCFST) (Hamidian et al., 2016). Hence, the benefits of using OCFST are higher for members subjected to flexural loading or for members with low D/t ratio, but, in general, the use of OCFST members is in vogue due to the enhancement of ductility in comparison with common reinforced concrete columns (Aslam et al., 2016b, 2017; Aslam et al., 2016c).

It is well known that OPBC behaves in a different and better way than NAC at elevated temperature, yet its performance is not completely known in case of confinement (Jumaat et al., 2015; Mohammadhosseini and Yatim, 2017). As lightweight aggregate concrete is more vulnerable to fire, therefore, it is necessary to evaluate the use of OPBC as infilled material in CFST. Despite the availability of numerous literatures on fire tests of steel columns filled with normal concrete, it is rare to find test results, which account for lightweight aggregate in CFST. Few studies can be found on the performance of different types of concrete filled in steel tube at ambient temperature (Chen et al., 2016; Silva et al., 2016). However, to date, no experimental and numerical study has evaluated the flexural behavior of lightweight concrete filled steel tube exposed to elevated temperature. Hence, in this paper, the results of an experimental program to evaluate the flexural behavior of novel oil palm CFST members subjected to elevated temperature are presented. The hollow steel tubes were filled with two different types of concrete namely NAC and OPBC. The thermal response, failure modes, critical temperature, temperature distribution in steel tube and infilled concrete, deflection along the span and fire concrete contribution ratio were evaluated. A new parameter i.e. fire concrete contribution ratio (FCCR) recently proposed by Romero et al. (2011) to enumerate the significance concrete infilling in steel sections subjected to elevated temperatures, was used to compare the effect of OPBS and NAC as infilled material. Thereafter, parametric study was conducted to evaluate the effect of different parameters (yield strength of steel, compressive strength of infilled concrete, load ratio, width-to depth ratio and steel ratio) on the FR time of CFST member. Finally, the experimental results were compared with existing equations available in literature for CFST columns filled with natural aggregate concrete.

2. Experimental Tests

2.1. Heating Arrangements/Setup

The elevated temperature experimental tests on square and rectangular CFST members were conducted at the Heavy Structures Laboratory of the University of Malaya, in Malaysia. Figure 1 shows different parts of the experimental test setup used in the elevated temperature tests of CFST beams. The setup consists of one vertical frame (1) and two horizontal “A frames” (2). The vertical 2D frame consists of 4.5m long beam. An ENERPAC hydraulic jack of 150 KN capacity in compression (3) was installed on the vertical 2D frame (1) and controlled by a hydraulic central unit (4). A load cell of 100KN (6) capacity was placed to monitor the applied load during the test. Beneath the load cell, a stub column (5) was placed to prevent the exposure of hydraulic actuator

to elevated temperature and to transfer the load from hydraulic actuator to the beam specimen. The specimen was placed inside the furnace and was supported by two small beams attached to horizontal A-frames, thus simulating simply-supported boundary conditions. For specimen heating, a horizontal electric furnace capable of replicating the ISO-834 fire curve (ISO 834:, 1999) was used. The dimensions of the internal chamber of the furnace were 2000mm (L) x 1000mm (W) x1000mm (H) while the length of specimen beam exposed to elevated temperature was 2 meters as shown in Figure 2. The experimental program consisted of 4 fire resistance tests, 2 of which were performed on NAC filled CFST (NCFST) while the remaining 2 were performed on OPBC filled CFST (OCFST). Both NCFST and OCFST samples were further demarcated as square and rectangular cross-section. The details of experimental program are summarized in Table 1. For all specimens, the steel ratio was kept constant while the nominal load ratio (n) was kept as 0.30. All specimens were labeled so that the types of beams could easily be identified. As an example, the sample ROCFST indicates a FR test on a rectangular OCFST beam.

Figure 1 General view of the experimental test setup

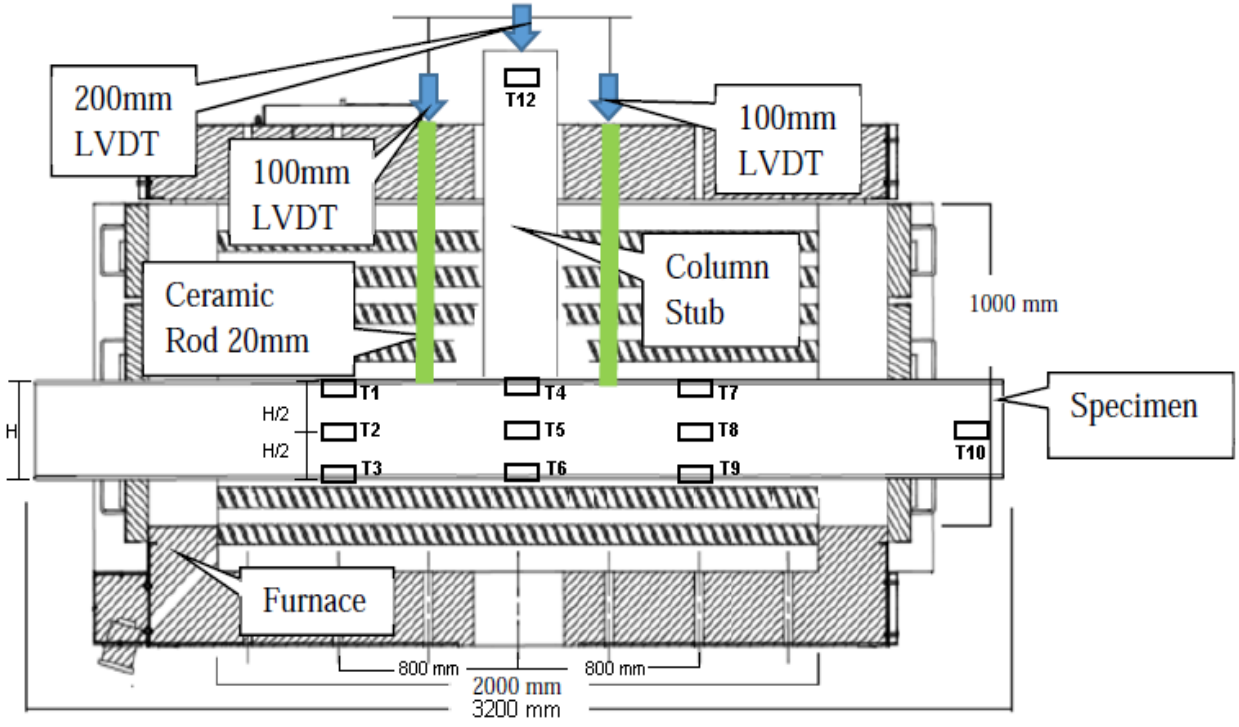

Figure 2 Location of thermocouples and side view of experimental setup

Table 1 Dimensions of tested specimens

Specimen Name	Height, H (mm)	Width, B (mm)	Thickness, t (mm)	Load Ratio, n	Cross-Sectional shape	Type of concrete
ROCFST	200.2	100.1	5.99	0.3	Rectangular	OPBC
RNCFST	200.4	100.1	6.01	0.3	Rectangular	Normal
SOCFST	150.8	150.8	5.99	0.3	Square	OPBC
SNCFST	150.7	149.9	5.99	0.3	Square	Normal

We would like to mention here that the length and the cross-sectional dimensions of steel selected for the experimental and parametric study are based on their availability in the market and recommendations of International code (LRFD, 1994). Various researchers have also used these dimensions in their experimental investigations. For example, in references (Jiang et al., 2013) the researchers used BxD as 150 × 150 and 100 x 200 with a length of 2000 mm. Also, the available experimental facilities and the testing setup were kept in mind while selecting the dimensions of the specimens.

2.2. Specimen fabrication

2.2.1. Steel

The steel tubes in all specimens were cold formed from steel plates by press bending and seam welding. The tubes were provided from a 12m length of hollow steel tube. Tensile tests were performed on steel coupons obtained from the original tubes. The 0.2% proof stress was adopted as recommended in literature for cold formed steel tubes (Yang and Han, 2006). The stress-strain curves for three coupon tests are shown in Figure 3. The measured yield strength, ultimate strength, elastic modulus and maximum elongation were found to be 394 MPa, 458 MPa, 201.3 GPa and 29%, respectively.

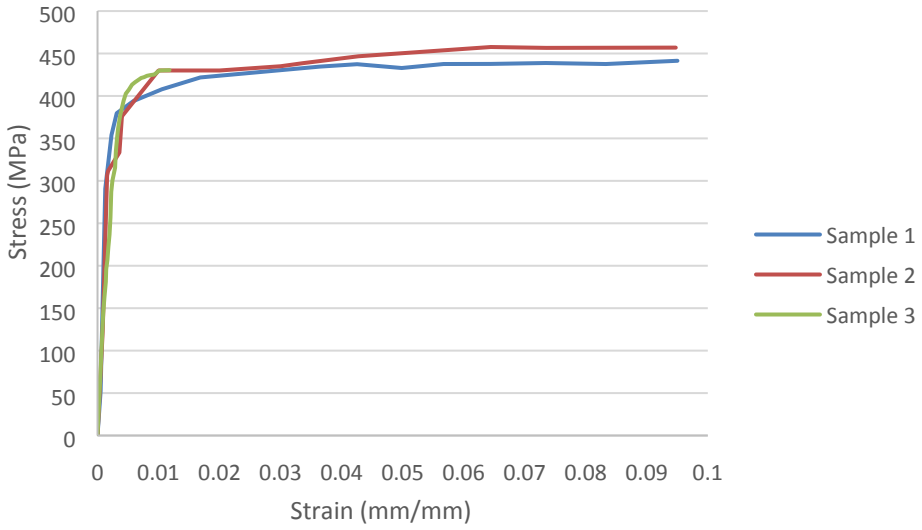

Figure 3 Stress-strain curves for tensile coupon tests

2.2.2. Concrete

Both NAC and OPBC (of Grade 50) were prepared in pan mixer. The steel tubes were then filled with concrete. A poker vibrator was used to vibrate and to remove entrapped air voids in concrete. The details of mix proportions are summarized in Table 2. The compressive strength of concrete was determined by testing 100 mm concrete cubes while the elastic modulus and stress-strain behavior of concrete was determined at 28 days by testing concrete cylinders having size of 150mm x 300mm. ISO 12570:2000 (ISO 12570:, 2000) was used to calculate the moisture content of concrete. The results of measured compressive strengths and elastic moduli of both types of concrete are presented in Table 3. It is important to mention here that although, these two concretes have similar compressive strength, but they have very different stress-strain behavior in compression as reported by numerous researchers (ACI Committee 318, 2015; Mustapa and Sulong, 2017; Nayaka et al., 2018).

Table 2 Mix proportions of NMC and OPBC concrete

Mix Type	Cement (Kg/m^3)	w/c	SP (%)	Granite CA (kg)	OPBC* (kg)	Sand (kg)	Slump (mm)
NMC	440	0.40	1.5	980	--	855	100
OPBC concrete	550	0.35	2	--	980	648	110

*OPBC aggregate was used in saturated surface dry condition in concrete

Table 3 Strength and Modulus of Elasticity at 28 days and time of testing

Type of Concrete Mix	F'c at 28 days (MPa)	Ec at 28 Days (MPa)	Density (kg/m^3)
NMC	52	31.2	2398
OPBC	51.2	32	2019

2.3. Measuring points arrangement

To obtain the temperature distribution along the length of each specimen, 10 type-K thermocouples were installed on steel tube as shown in Figure 2 while one thermocouple was embedded at the mid-height of concrete to measure the temperature of infilled concrete (T11). In order to measure the temperature of the furnace, 4 type-K thermocouples (T13-T16) were embedded at different locations in the furnace. The thermocouples readings were recorded with the help of the assembly attached to the furnace. Three Linear Variable Differential Transformers (LVDTs) were placed on the top-side of specimen to measure the deformation of the specimen under elevated temperature. The detailed arrangement of thermocouples and displacement transducers is shown in Figure 2. A TDS-530 data logger was used to record the readings from load cell and LVDTs at every second.

2.4. Test Plan

The elevated temperature tests were conducted under transient state heating conditions to replicate the real-life scenarios. In transient state test, the sample is loaded to some stress level by applying load statically. Thereafter, the temperature is increased gradually by using different standard fire time-temperature curves recommended by various testing methods, until failure point (Javed, M.F. et al., 2017a).

The experimental test comprised of two basic stages; loading stage and heating stage. For the loading stage, the applied load ratio was selected as 30% of the design value at room temperature because it replicates the common serviceability load of a CFST flexural member of real building structures (Rodrigues and Laim, 2017; Rodrigues and Laím, 2017). The design value was calculated using Chinese code (GB50936, 2014). During the loading stage, the flexural load was applied to the specimens 30 min. before igniting the furnace. The specimen was loaded gradually at a rate of 2.5mm/min. When the load reached the desired level, it was maintained for a period of 2 minutes. During the second stage, the furnace was ignited, and the beam was exposed to elevated temperature such that, the average temperature of the furnace corroborated the ISO 834 fire curve closely. It is noteworthy that the room temperature was 27°C at the time of igniting the furnace.

3. Test Results and Discussion

3.1. Thermal response

3.1.1. Furnace Temperature vs ISO-834 curve

The comparison of the average temperature of the furnace (T13-T16) and ISO-834 curve is shown in Figure 4. The furnace temperature is lower than ISO-834 curve at the start of the test. This kind of delay is common in electric furnace and has been reported by several researchers (Craveiro et al., 2016; Romero et al., 2011). The amount of delay is directly related to size of furnace (Albero et al., 2016; Espinos et al., 2013; Ibañez et al., 2016; Wan et al., 2017). At 15 minutes, the difference ranged between 10% and 20%. Similar difference was reported at 15 minutes by different researchers and is deemed acceptable (Laím et al., 2016; Rodrigues and Laim, 2017; Rodrigues and Laím, 2017). The reason for evaluating the difference at 15 minutes is associated with the fact that complete furnace is heated properly and the effect of type of furnace and heating media is uninvolved (Huo et al., 2015; Sauca et al., 2016). Furthermore, the temperature of the furnace is similar for different size and shape of specimen.

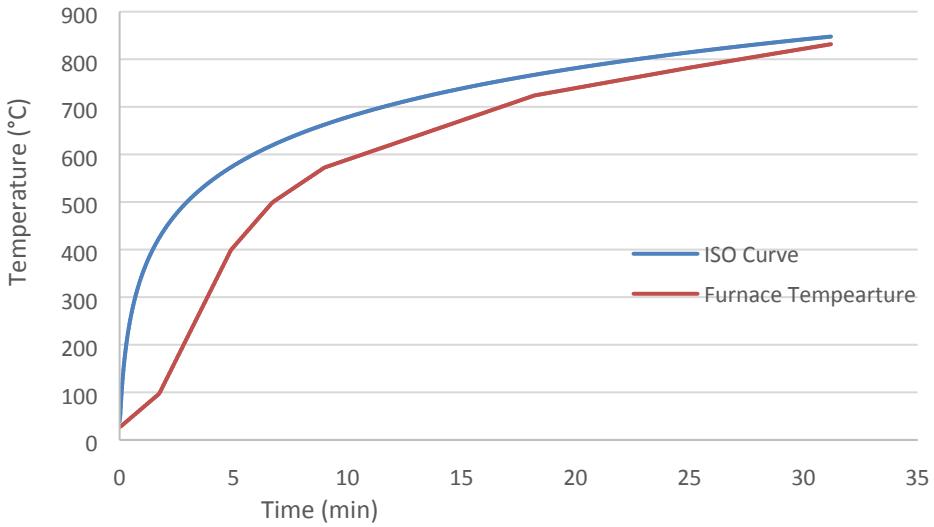

Figure 4 ISO-834 and furnace temperature throughout the test

3.1.2. General response of tested specimen

The evolution of temperature in one of the tested specimen, SNCFST can be observed in Figure 5. The temperature measured by the thermocouples installed on the outer steel tube (T1-T9) lie close to each other while the temperature measured by thermocouple installed at concrete core (T11) is significantly lower than outer steel temperature. T10, installed closer to the support of the beam and being outside the furnace, registered the lowest temperature in beginning of the test and reached maximum value of 130°C and then stopped till end of the test. The thermal response of the rest of the specimens was similar except that the infilled concrete observes lower temperature in OCFST.

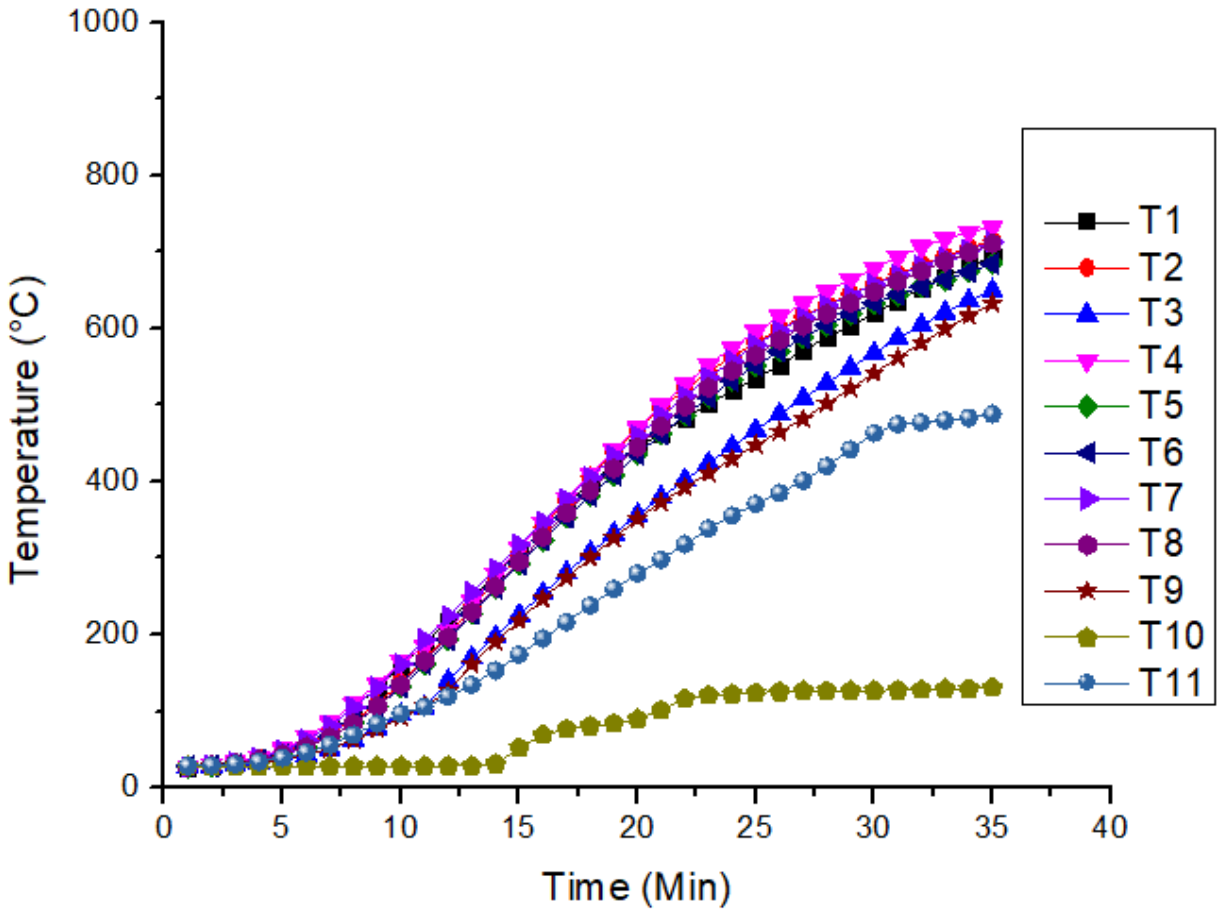

Figure 5 Temperature distribution in SNCFST

3.1.3. Effect of type of infilled concrete

Figure 6 shows the comparison of temperature of infilled concrete of all four specimens. At 30 min, the temperature of the concrete in OCFST is almost 100˚C less than NCFST. The better performance of OCFST is due to the porous nature and low thermal conductivity of OPBC aggregate. Moreover, OPBC is prepared at a high temperature (850°C). The results obtained are in line with available literature (Jumaat et al., 2015), where they showed that for the same duration of exposure to fire, the temperature of OPBC is less than NAC. Figure 7 shows the comparison of outer steel tube temperature of SNCFST and SOCFST. At 30 minutes, the temperature of steel tube of OCFST is 50°C lower than steel temperature of NCFST. Thus, based on the temperature of steel tube and infilled concrete temperature, it can be concluded that OCFST performs better than NCFST at elevated temperature.

231

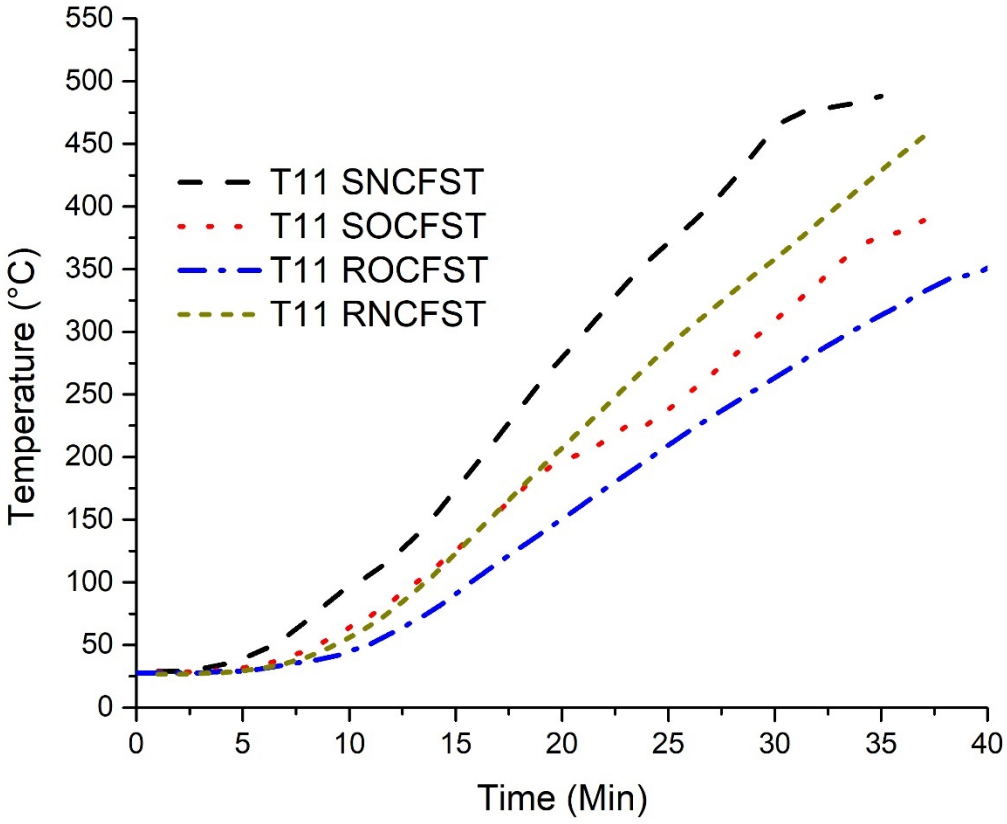

232
233 Figure 6 Temperature of infilled concrete of all specimens

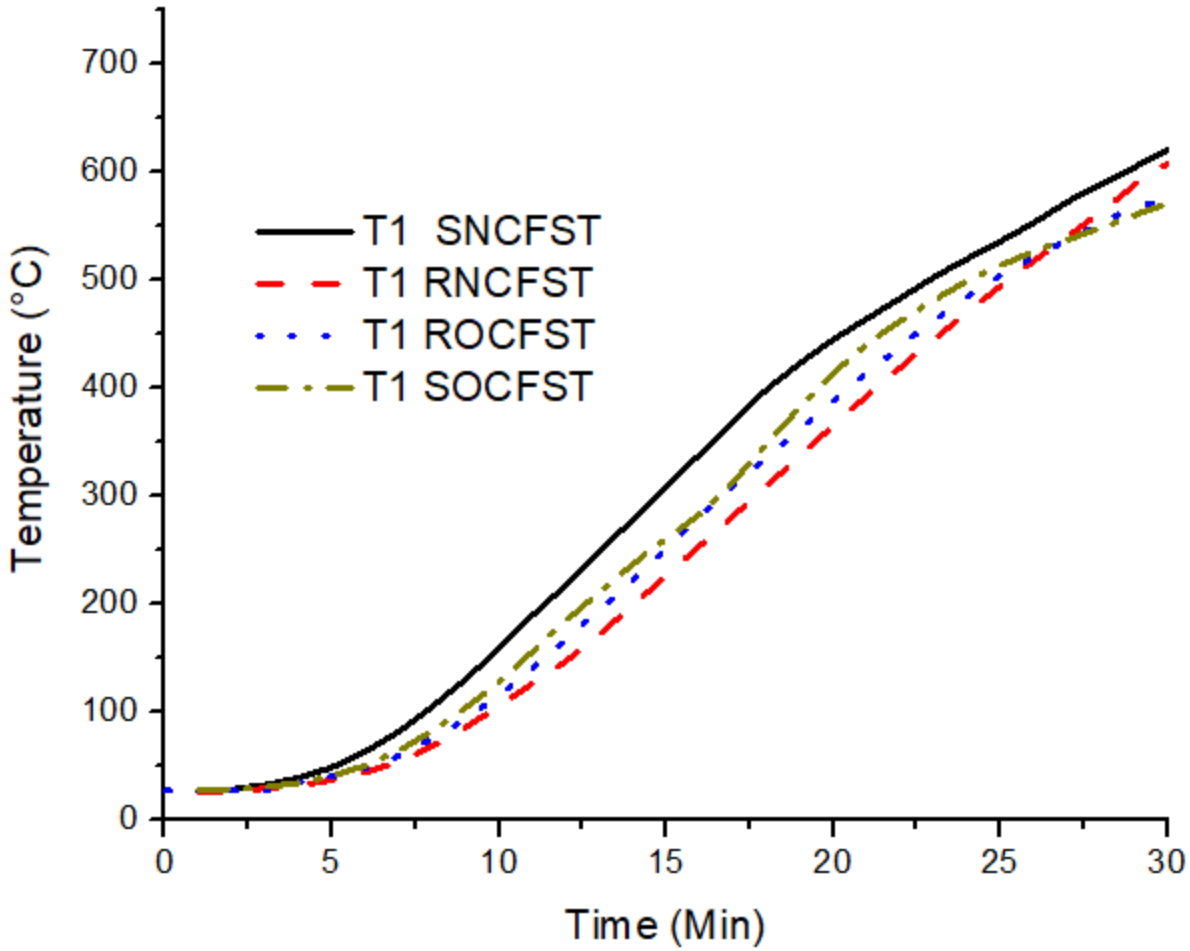

Figure 7 Temperature of steel tube of all the specimens

3.1.4. Effect of Cross-sectional shape

Figure 8 shows the comparison of temperature evaluation in steel tube and infilled concrete for SOCFST and ROCFST. The rate of rise of temperature in steel is same for both square and rectangular beams whereas the rate of rise of temperature of infilled concrete in square CFST is higher than rectangular CFST. The reason for this may be the availability of larger amount of area at the end of the tube for square CFST (12% larger) than rectangular CFST, which in turn, resulted in the escape of moisture.

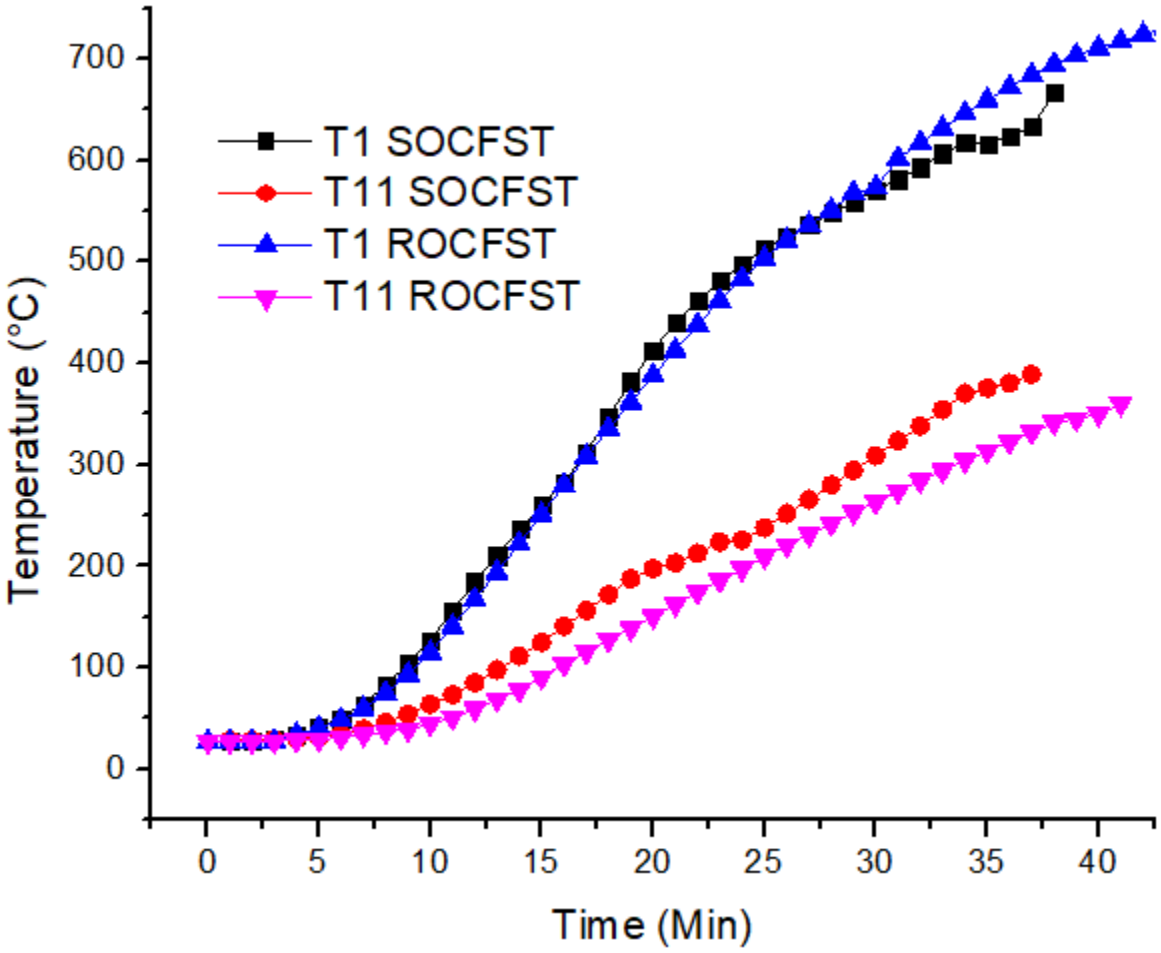

Figure 8 Comparison between the temperature of infilled concrete and steel tube of SOCFST and ROCFST

3.2. Failure modes

Figure 9 shows the displacements of square and rectangular NCFST members at different time duration of the test. As the beam boundary and loading conditions were symmetrical, the deformation of the specimens was also observed to be symmetrical. The displacement increased rapidly with the increase in temperature of the member for constant load level especially between 25 min to 30 min. This rapid increase is due to the yielding of steel. The results of the tests performed in this study are presented in Figure 9. At any time interval, the deflection in rectangular cross-section is less than the square cross-section. The reason for the better performance of rectangular cross-section is its higher moment of inertia as compared to square cross-section. It is important to mention that although the load ratio for all the specimens was kept constant i.e., 0.3, the amount of load applied on rectangular cross-sections is greater than the load applied on square cross-section as shown in Table 4.

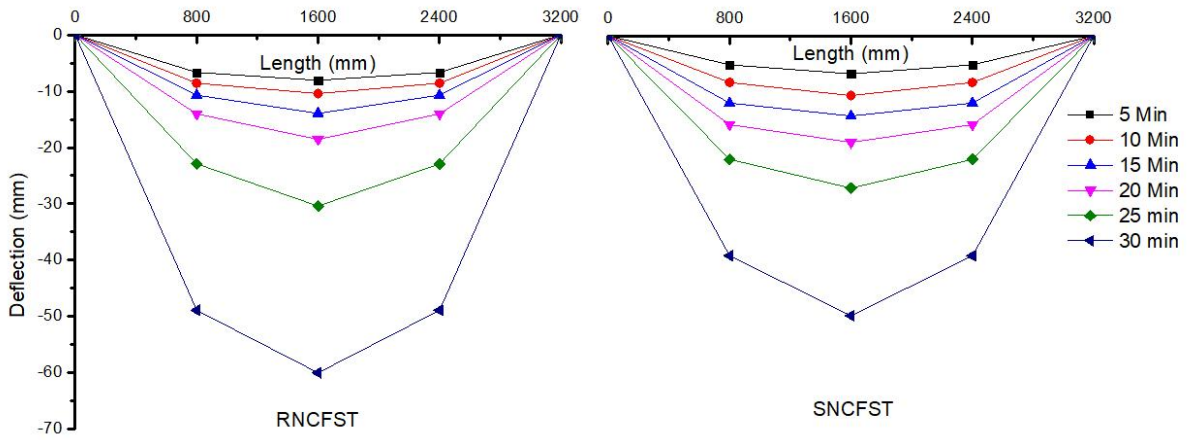

Figure 9 Deflection of RNCFST and SNCFST beam at different time intervals

Figure 10 shows the deflection of different points in SOCFST and SNCFST at different time interval. At any instance of time, the deflection in SNCFST is much higher than SOCFST showing the superior structural behavior of SOCFST. As mentioned before, this is due to the low temperature of infilled concrete causing the slower loss of strength due to elevated temperature. For constant load level, the displacement increases rapidly with an increase in temperature of the member especially between the last 5 minutes of the test due to the yielding of steel.

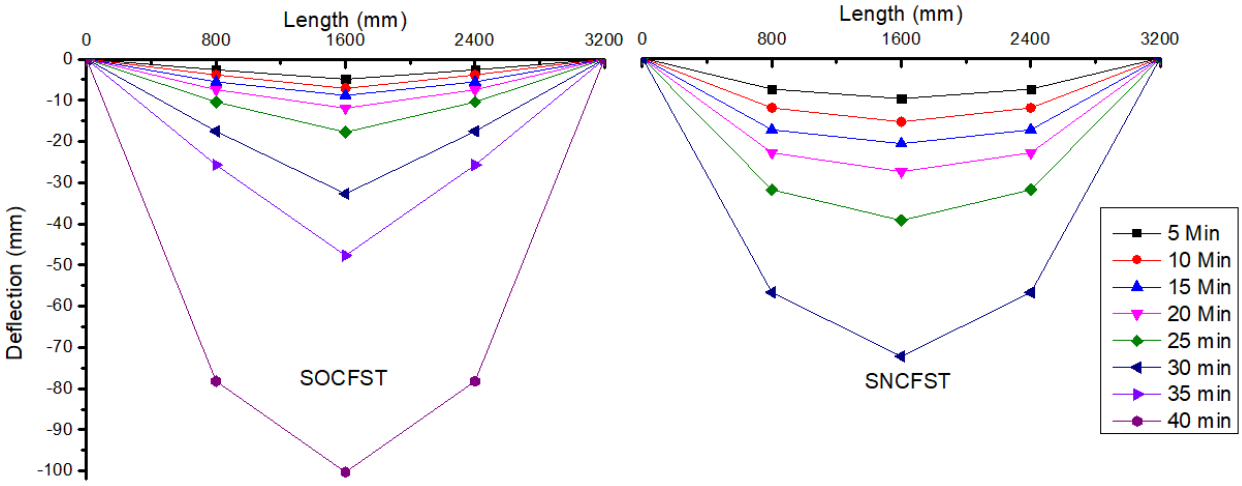

Figure 10 Deflection of SOCFST and SNCFST beam at different time intervals

The typical failure mode observed for all the specimens was global buckling. Figure 11 shows RNCFST and ROCFST after failure. The absence of local buckling shows that the hollow steel tubes were properly filled with concrete. No tensile fracture was observed on the tension flange. The evolution of mid-span deflection versus the fire exposure time was determined during the fire tests and is presented in Figure 12. The failure pattern showed ductile behavior, which is attributed

to the ductility and shear contribution of outer steel tube. Specimens retained their integrity after testing. These observations are strong evidence pointing towards the interaction of the concrete and steel in the CFST beams during the whole process of fire exposure. It must be noticed that due to flexural load and combined with low tensile strength of concrete, there is no plateau in these curves. The plateau in deflection versus time is commonly observed in CFST columns with high slenderness and is due to the contribution of infilled concrete (Moliner et al., 2013; Romero et al., 2011). It is important to mention at this point that majority of CFST columns when exposed to fire failed due to crushing of concrete while in this case the failure was due to the yielding of outer steel tube. According to available literature (Rush et al., 2011), the mode of failure of CFST members depends on many factors including slenderness ratio, applied load, type of load, load ratio and type of support conditions. It can be concluded that the structural response of square and rectangular beams is similar throughout the test until failure. The slope of time-deflection curve shows the initial flexural stiffness of member. It can be concluded that the SOCFST performs better than SNCFST at elevated temperature. Similarly, rectangular cross-sections perform better than square cross-sections for members subjected to flexural loads.

Figure 11 Failure modes of RNCFST and ROCFST

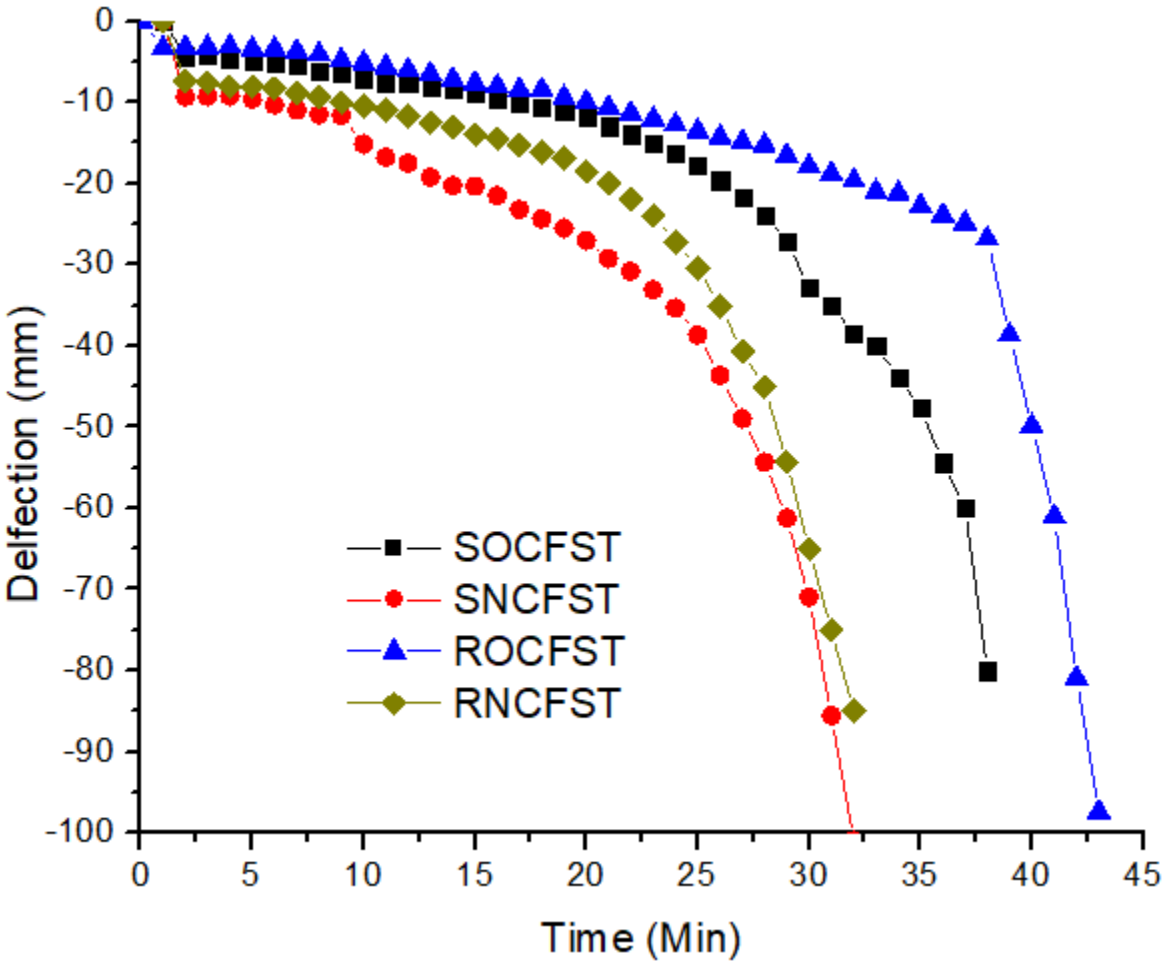

Figure 12 Mid-span deflection vs time of all specimens

3.3. Critical Temperature/ Limiting Temperature

The temperature corresponds to the deflection $L_e/50$ is taken as the critical temperature of the specimen. The definition of critical temperature is used to ease the evaluation of the fire performance of steel members (de Normalisation, 1994; Franssen and Real, 2016; Tubes). This definition may also be used into the evaluation of the fire performance of CFST members. Table 4 shows the critical temperature measured at the middle (average of T5, T6 and T7) of the specimen. It is evident that the higher value of limiting temperature shows its tendency for higher fire resistance and towards the fact that the limiting temperature can reflect the fire behavior and resistance of the test specimens. The critical temperature of OCFST is 30°C more than NCFST for both square and rectangular cross-sections. Thus, it can be concluded that the type of infilled concrete affects the rate of heating and critical temperature of the CFST. This finding is not in line with the conclusions drawn by (Lu et al., 2009; Moliner et al., 2013), who found that the critical temperature of CFST columns was not affected by the type of infilled concrete. The difference in results is due to the lower slenderness of the specimens tested in this experimental program while

the slenderness of the specimens available in literature (Lu et al., 2009; Moliner et al., 2013) was more, therefore making it impossible to gain advantage of the type of infilled concrete.

The prediction using the limiting temperature method for FR of CFST specimens is more complicated than that for the steel ones because of the non-uniform thermal distribution of the cross-section induced by the infilled concrete core (Yang et al., 2013). The critical temperature obtained from the experimental tests is also compared with the values obtained by equation 1. Equation 1 is given in EC3 for the calculation of critical temperature of CFST columns resisting some percent of design axial load.

$$T_{cr} = 39.19\ ln\left(\frac{1}{0.9674\mu^{3.833}} - 1\right) + 482 \qquad \text{Equation 1}$$

Where μ is the load ratio and T_{cr} in °C is the critical temperature of the specimen exposed to standard fire.

Table 4 Critical temperature of the tested specimens

Specimen	Applied Load, KN	Load Ratio, Hollow	T_{cr} Experimental, °C	T_{cr} code hollow, °C	T_{cr} code, °C
ROCFST	38	0.5	756	584.66	663.77
RNCFST	38	0.5	722	584.66	663.77
SOCFST	30	0.445	718	604.98	663.77
SNCFST	30	0.445	685	604.98	663.77

Two values were calculated with this method of the limiting temperature corresponding to: T_{cr} code hollow and T_{cr} code. The value for hollow section is calculated because in some cases the steel tube fails before utilizing the infilled concrete. As shown in Table 4, the values obtained from the equation given by EC3 are close to critical temperature obtained for SNCFST from experimental test. However, the difference in predicted values and experimental values are 50°C or greater for all the other samples. Hence, the equation given by EC3 needs to be revised and it is recommended to include the effect of different types of infilled concrete and cross-sections.

3.4. Critical Time

The time corresponds to critical temperature is termed as critical time. Figure 13 shows that critical time for ROCFST and SOCFST is more than RNCFST and SNCFST members by 10 and 7 minutes, respectively. The enhancement is more in rectangular cross-sections as compare to square cross-sections. Several researchers (Laím et al., 2016; Rodrigues and Laim, 2017; Rodrigues and Laím, 2017) investigated and compared critical times of circular, square, rectangular and elliptical CFST members subjected to axial load and concluded that the critical time of elliptical CFST is highest followed by circular, rectangular and square CFST columns respectively. It was also found that the maximum difference in critical time was less than 15%. Thus, based on critical time, it can be concluded that OCFST performs better than NCFST at elevated temperature.

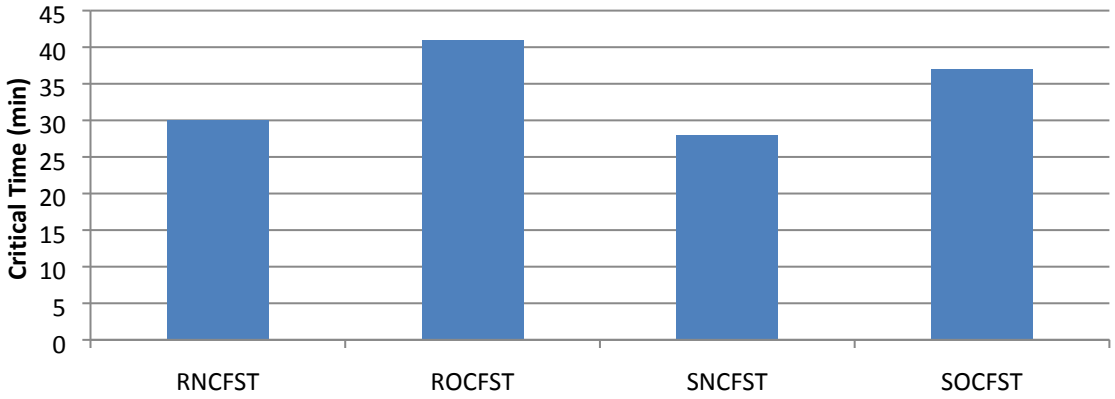

Figure 13 Critical time of the tested specimens in min

3.5. Fire concrete contribution ratio (FCCR)

To assess the importance of filling concrete in hollow steel tube beams exposed to fire and to study the interest of using different types of concrete, fire concrete contribution ratio (FCCR) is used by different researchers (Moliner et al., 2013). FCCR is the ratio of FR rating of CFST and that of the hollow member, both subjected to the same amount of flexural load. (Moliner et al., 2013)

$$FCCR = \frac{FR_{Filled}}{FR_{Hollow}} \qquad \text{Equation 2}$$

In the above equation FR_{Filled} and FR_{Hollow} is the FR time of filled CFST and hollow steel tube. FR_{Filled} can be calculated numerically or experimentally, but FR_{Hollow} can be obtained numerically by using equations available in literature (Yu et al., 2014). Table 5 presents the FCCR obtained for the series of tested specimens, which represents the gain in the FR period by using concrete-filled members instead of hollow steel members. In Table 5, it can be observed that for the same amount of steel and load ratio, the FR of rectangular section is 30% higher than square cross-section for tubes filled with NMC. Similarly, the FCCR of OCFST is 30% higher than NCFST. Hence, cross-sectional shape of steel tube and type of infilled concrete greatly affects the FCCR despite having same compressive strength. It is concluded that the FR of a hollow steel member can be enhanced at least 1.5 to 2.5 times by concrete infilling. Similar conclusions were found for CFST columns by (Moliner et al., 2013). Based on FCCR, it can be concluded that the OCFST structural performance is better than NCFST at elevated temperature.

Table 5 Fire concrete contribution ratio of all tested specimens

S.No	Specimen	FR CFST	Load Ratio, Hollow	FR hollow	FCCR
1	ROCFST	41	0.5	16	2.56
2	RNCFST	30	0.5	16	1.88
3	SOCFST	37	0.445	20	1.85
4	SNCFST	28	0.445	20	1.40

4. FE Modeling

4.1. Model Description

The modelling and analysis were performed in commercially available FE software ANSYS. The total length of the simply supported beam was 3200 mm, where only the central part of length 2800mm was exposed to fire. The temperature of beam specimen was kept uniform in the fire exposed area. The applied load was kept constant while the temperature was increased according to ISO-834 curve. For this study, 3D quadrilateral reduced integration solid element was used to model the infilled concrete while 3D hexahedral reduced integration solid element was used to model the outer cold formed steel tube. Mesh convergence study was performed to select the reasonable number of elements and its size. A surface-based interaction with a Coulomb friction model and hard contact pressure model in the tangential and normal direction, respectively were used to model the interface between steel and concrete core. The friction factor was taken as 0.6 (Javed, M. et al., 2017; Javed, M.F. et al., 2017b). The details of beam and application of load and support conditions are shown in Figure 14 and Figure 15, respectively.

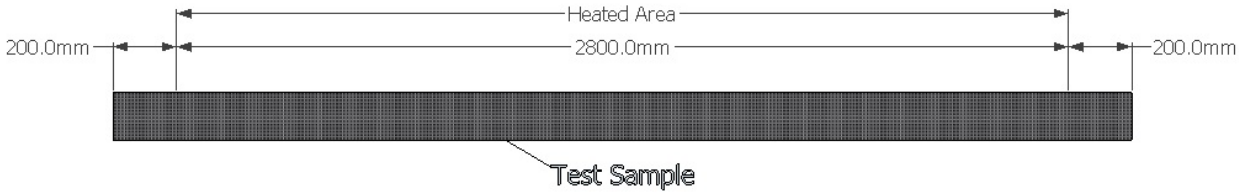

Figure 14 Test sample showing heated length of specimen

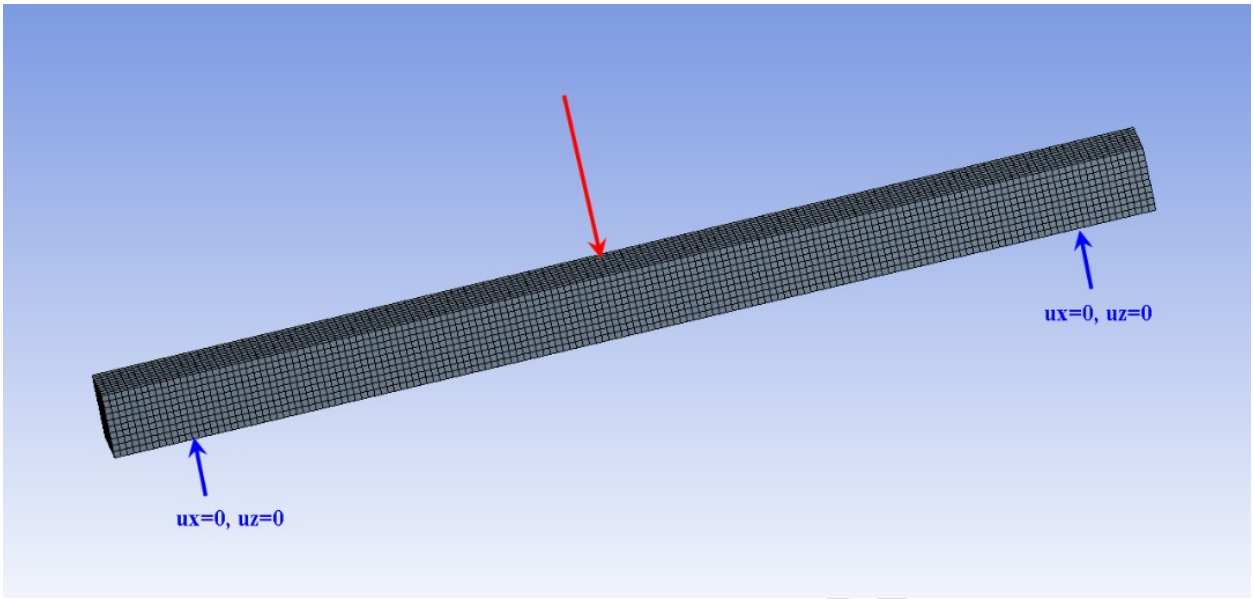

Figure 15 FE model with load applied and support conditions

4.2. Thermal Analysis

Thermal analysis was performed on the developed FE model with the help of heat transfer option in ANSYS. Table 6 shows the values of different parameters used in thermal analysis. The values of different governing parameters like constant convective co-efficient for exposed and unexposed surface, steel emissivity value and radiative heat flux were used according to EC1(EN, 1991). Thermal conductivity and specific heat of normal concrete and steel were calculated according to EC2 (EN, 2004) and EC3 (CEN, 2006), respectively. For thermal expansion co-efficient of steel and concrete, the values recommended by Hong and Varma (Hong and Varma, 2009) were used.

Table 6 Properties of steel and concrete used in FE model

Parameters	Values
constant convective co-efficient for exposed surface	25 W/m^2 K
constant convective co-efficient for unexposed surface	9 W/m^2 K
Steel emissivity value	0.8
Stefan–Boltzmann constant	5.67 x 10^{-8} W/m^{2}K^4
Thermal expansion co-efficient for steel	12 x 10^{-6}/°C
Thermal expansion co-efficient for concrete	6 x 10^{-6}/°C

4.3. Material constitutive models

The degradation of mechanical and thermal properties related to temperature were adopted. For steel, the model proposed by Espinos (Espinos, 2012) was employed. As Poisson's ratio is not affected by temperature, so it is assumed to be 0.3. The strength reduction factors were used to calculate the yield stress and elastic modulus at elevated temperature respectively (Kesawan and Mahendran, 2018; Li and Young, 2017). The stress-strain curves for fy= 394 MPa obtained from

the model used for different temperatures are shown in Figure 16. For concrete, the constitutive model presented by Han et al. (Han et al., 2003) was employed, as this model take into account the effect of bonding between concrete and steel. Previous studies show that the inclusion of slip between concrete and steel interface has very minor effect on the FR time of CFST member (Ding and Wang, 2008), hence, it was not included in the current FE model.

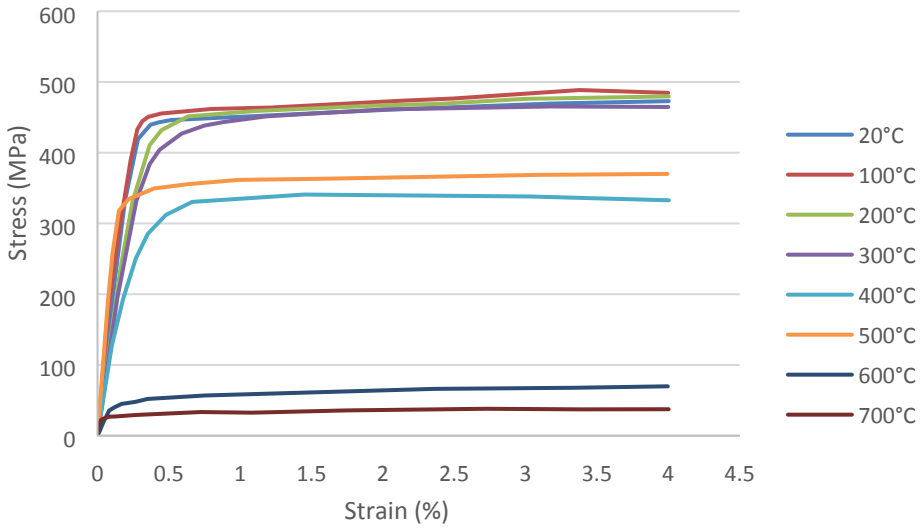

Figure 16 Stress-strain curves for fy=394 MPa steel at different elevated temperatures

4.4. Initial geometric imperfection and amplitude

Different researchers recommended different initial geometric imperfection values for CFST (Han et al., 2013; Tao et al., 2009; Wang and Young, 2013). In this study, imperfections in the form of lowest global elastic buckling mode were included. Since the geometric imperfections were not calculated at the time of experiment, three assumed values of imperfections were considered for the initial geometric imperfection sensitivity analysis (Khan et al., 2018; Khan et al., 2017). Figure 17 shows the comparison of time deflection curves between experimental data and FE model having different values of imperfections. It can be seen that smaller imperfections resulted in higher FR time but significantly decreases the computation time. The imperfection value of L/2000 gives the most favorable comparison, where L is the total length of the beam specimen. This value of L/2000 was used by Han et al. (Han et al., 2013) for stainless steel tubes. Hence, based on results of Figure 17, the initial geometric imperfection value of L/2000 was used in verification and parametric studies.

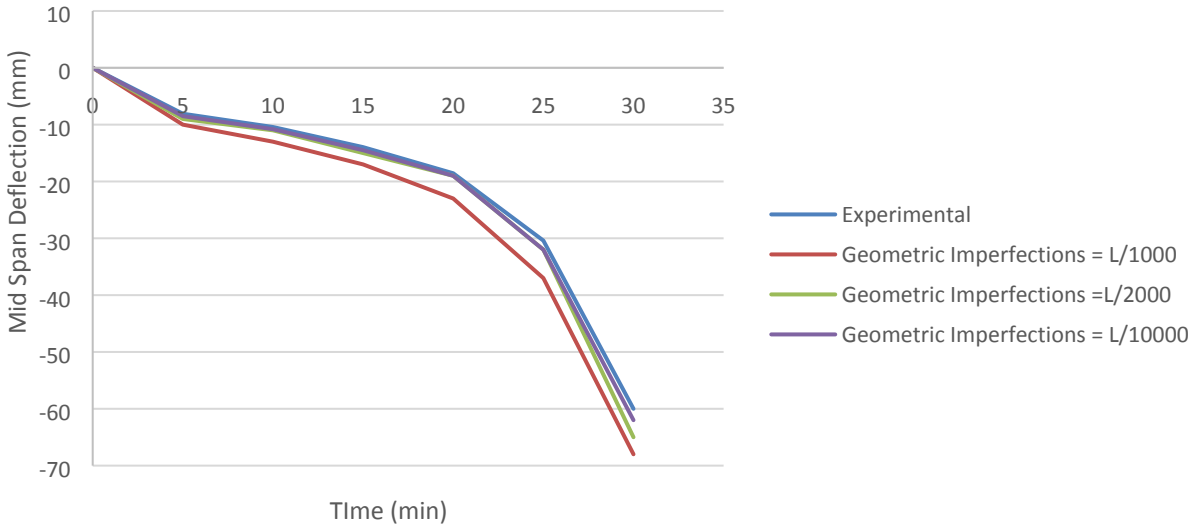

411

412 Figure 17 Mid-span deflection of different experimental tests and different FE models with
413 different initial imperfections

414 ## 4.5. Verification of FE model

415

416 The temperature of steel tube and infilled concrete and mid-span deflection obtained from the
417 experimental tests and FE model were compared for verifying the FE model. Figure 18 shows the
418 time-temperature curve of outer steel tube of one rectangular and one square CFST beams. The
419 difference between experimental and FE model results for outer steel tube is negligible after 15
420 min. At the start of the test, the temperature predicted by FE model is higher than experimental
421 values. However, it gets accurate at the end of the test. This may be due to the usage of electric
422 furnace for experimental tests as explained in section 3.1.1.

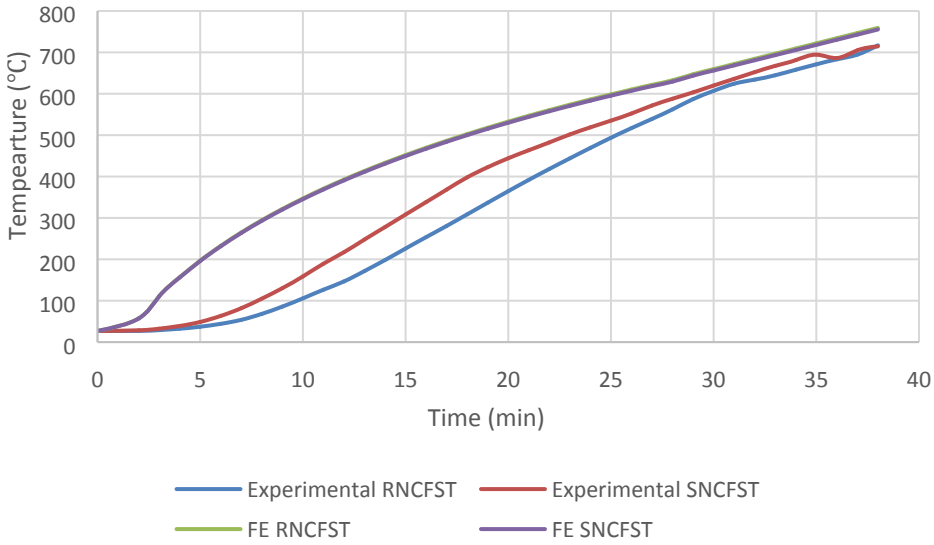

423

424 Figure 18 Comparison of experimental and FE model time-temperature curve for outer steel tube

425 The mid-span deflection obtained from FE model and the measured mid-span deflections during
426 test are compared for square and rectangular beams as shown in Figure 19. Some minor difference
427 between experimental and FE model results can be observed. Such kind of small differences were
428 reported by many researchers for CFST members at room and elevated temperatures (Chung et al.,
429 2009; Espinos, 2012; Javed, M.F. et al., 2017b). The FR time obtained from experimental results
430 and FE model are presented in Table 7. The close resemblance of experimental and FE model
431 results shows that the co-efficient of thermal expansion used for concrete, steel and steel-concrete
432 interface are accurate and can be used for future research works. The mean, standard deviation and
433 COV for the ratio between experimental and FE model results are 1.02, 0.025, and 2.45%,
434 respectively. The displacement predicted by FE model at the time of failure was less than the
435 experimentally measured displacement as shown in Figure 19. This may be due to neglecting the
436 "creep effect" in the FE model as the "creep effect" is enhanced at elevated temperature (Abid et
437 al., 2017; Han et al., 2001).

438

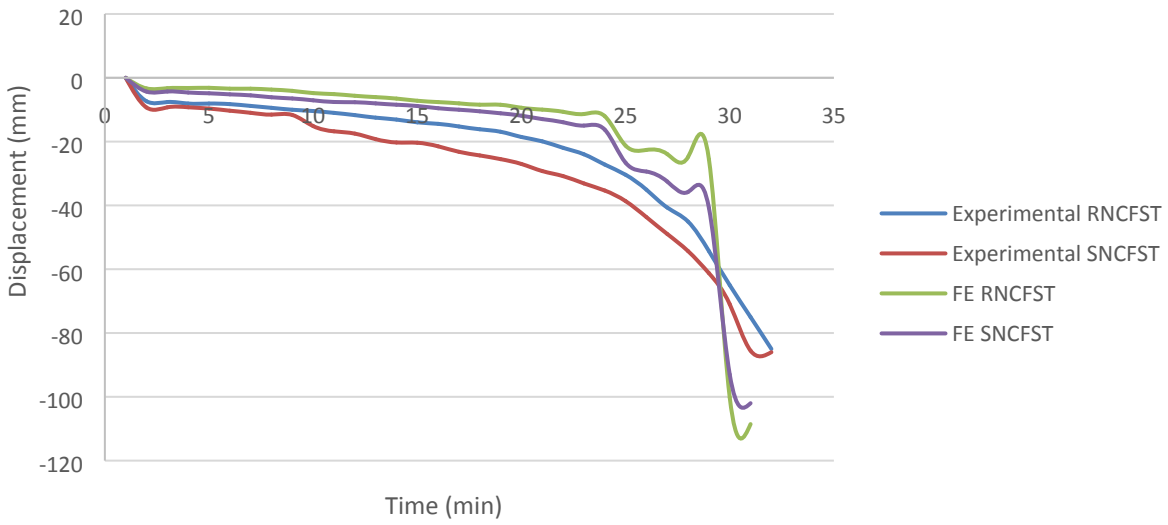

Figure 19 Time vs displacement curve for experimental and FE models

Table 7 FR time for experimental and FE models

Specimens	FR time, min (Exp)	FR time, min (Num)	Exp/Num
SNCFST-1	28	27.5	1.02
SNCFST-2	28.5	27.2	1.05
RNCFST-1	29.5	29.25	1.01
RNCFST-2	29	29.25	0.99
Mean			1.02
Standard Deviation			0.025
COV (%)			2.45

5. Parametric study

In this section, more than 50 CFST specimens were analyzed with the help of verified FE model. The dimensions and details of the analyzed specimens are given in Tables 8-11, where D, B, t, fy and fu represents the depth, width, thickness, yield strength and ultimate yield strength of steel section, respectively while Fc and n represents the compressive strength of concrete and load ratio, respectively. Most of the dimensions of the beam considered in this parametric study are same as already presented in (Javed, M.F. et al., 2017b), as these dimensions are most widely used in practical applications.

5.1. Effect of yield strength of steel

The main objective of this parametric study was to evaluate the effect of different yield strengths of steel on the FR time of CFST members when exposed to elevated temperature and flexural loads. For this purpose, five different values of yield strengths were considered. As changing the

yield strength of steel may affect the FR time differently for different compressive strength, load ratio and cross-sectional dimensions, therefore 20 models were analyzed. The modulus of elasticity of steel and concrete were assumed as 200 GPa and 29 GPa, respectively. The detailed dimensions of the FE model considered are shown in Table 8 while the rest of the parameters were same as mentioned in section 2.

Table 8 Main properties for CFST models used for studying the effect of yield strength of steel

Group Name	D × B × t	f_y (MPa)	f_u (MPa)	Fc (MPa)	Load ratio, n	FR Time (min)
Fy1	300x150x5	235	380	30	0.3	44.7
		275	410			41.2
		300	430			35.6
		355	450			28.84
		400	490			22.35
Fy2	300x150x5	235	380	30	0.6	36.8
		275	410			32.14
		300	430			25.64
		355	450			20.4
		400	490			15.824
Fy3	300x150x5	235	380	60	0.3	61.2
		275	410			57.1
		300	430			50.6
		355	450			44.7
		400	490			42.228
Fy4	300x600x5	235	380	30	0.3	91.6
		275	410			82.46
		300	430			73.51
		355	450			64.17
		400	490			54.96

Figure 20 shows the influence of yield strength of steel on the FR time of CFST members subjected to flexural load only. It can be seen in Figure 20 that increase in yield strength of steel causes decrease in the FR time of CFST beam regardless of load ratio, compressive strength of concrete and cross-sectional dimensions. By increasing the yield strength of steel from 235 MPa to 300 MPa and 400 MPa, the FR time of Fy1 group was found to decrease by 21% and 50%, respectively. The strength degradation with increasing yield strength is similar for different load ratios. However, for FY4 group having larger cross-section, higher load ratio and lower concrete strength, the decrease in FR time was higher. Since in larger cross-sections with low strength infilled concrete, steel takes majority of the load, and once steel losses its strength, the member fails quickly. While in case of smaller cross-sections and high strength of infilled concrete as in group Fy3, higher amount of load is taken by concrete, hence it is less affected by the yield strength of steel. It should be kept in mind that for constant load ratio, the load taken by high strength steel was more.

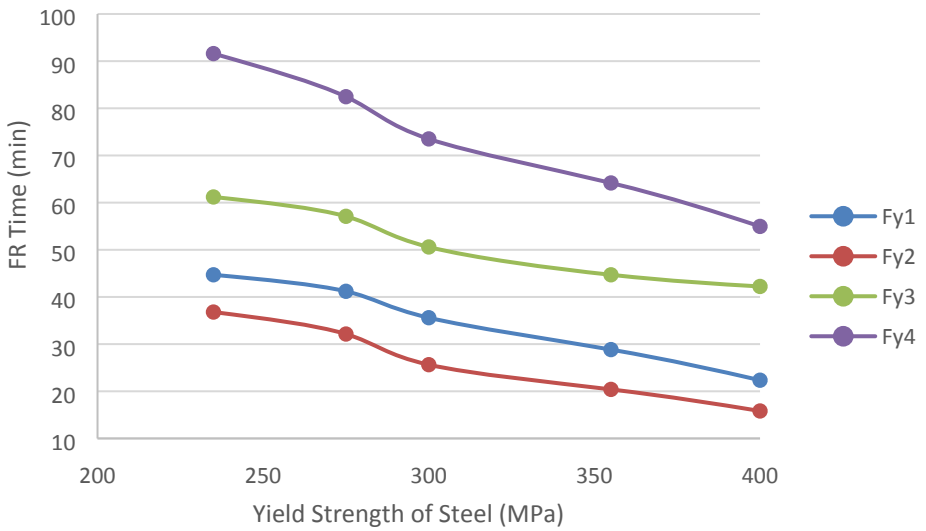

473

474 Figure 20 FR time values for different yield strengths of steel

475 ## 5.2. Effect of strength of concrete

476 To study the influence of compressive strength of infilled concrete on the flexural behavior of
477 CFST member at elevated temperature, 3 different compressive strengths of concrete were
478 considered. As varying compressive strength of concrete may affect the FR time differently for
479 different yield strength of concrete and cross-sectional dimensions, therefore 18 models were
480 analyzed for this section. The modulus of elasticity of concrete was calculated by using the
481 equations suggested in ACI-318 (ACI Committee 318, 2015). The rest of the parameters were kept
482 constant so that the effect of compressive strength is highlighted. The detailed dimensions of the
483 FE model considered are shown in Table 9 while the rest of the parameters were same as mentioned
484 in section 2.

485 Table 9 Details of models used to study the effect of compressive strength of concrete

Group Name	D × B × t	f_y	fc	n	FR Time
Fc1	300x150x5	235	30	0.3	44.7
			60		61.2
			75		70.15
Fc2	300x150x5	275	30	0.3	41.2
			60		57.1
			75		65.2
Fc3	300x150x5	400	30	0.3	22.35
			60		42.23
			75		50.57

Fc4	300x600x5	235	30	0.3	91.6
			60		98.4
			75		110.74
Fc5	300x600x5	275	30	0.3	82.46
			60		92.7
			75		99.32
Fc6	300x600x5	400	30	0.3	54.96
			60		64.02
			75		70.25

Figure 21 shows the effect of compressive strength of concrete on FR time for various yield strengths of steel and different cross-sections. By increasing the compressive strength of infilled concrete, the FR time increased regardless of the size and yield strength of steel tube. By increasing the compressive strength of infilled concrete from 30 MPa to 60 MPa and 75 MPa, the FR time of Fc1 group was found to increase by 37% and 57%, respectively. In can also be seen that the percentage increase in FR time is less for larger cross-sections. For instance, by increasing the compressive strength of infilled concrete from 30 MPa to 60 MPa and 75 MPa, the FR time of Fc4 group was found to increase by only 7% and 21%, respectively. Similar conclusions were made by researchers for concrete filled stainless steel members subjected to axial load at elevated temperature (Han et al., 2013).

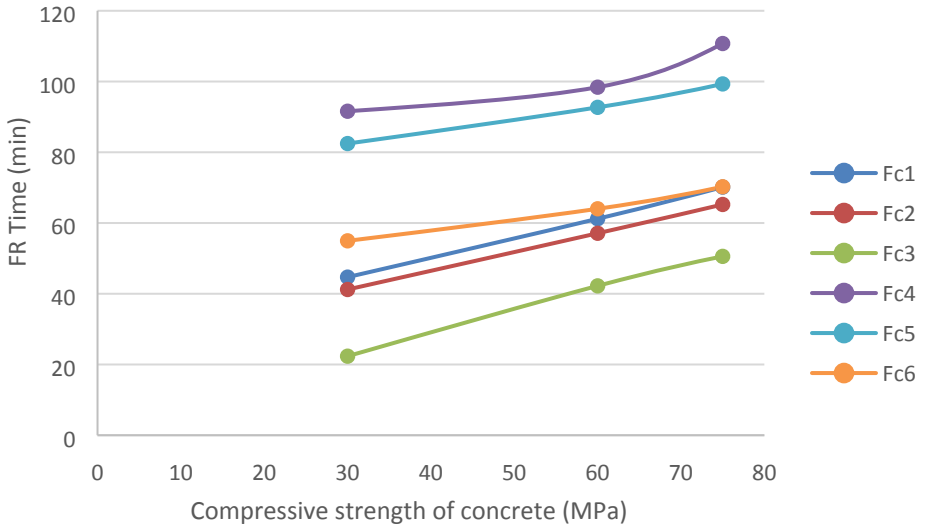

Figure 21 FR time of beams for different compressive strengths of concrete

5.3. Effect of load ratio

To study effect of load ratio on the elevated temperature performance of CFST members subjected to flexural members, three different load ratios were selected. As varying load ratio may affect the FR time differently for different yield strength of steel, therefore 15 models were analyzed. The detailed dimensions of the FE model considered are shown in Table 10 while the rest of the parameters were same as mentioned in section 2.

Table 10 Main properties for CFST models used for studying the effect of load ratio

Group Name	D × B × t	f_y	fc	n	FR Time
LR1	300x150x5	235	30	0.3	44.7
				0.45	40.87
				0.6	36.8
LR2	300x150x5	275	30	0.3	41.2
				0.45	35.26
				0.6	32.14
LR3	300x150x5	300	30	0.3	35.6
				0.45	29.21
				0.6	25.64
LR4	300x150x5	355	30	0.3	28.84
				0.45	25.51
				0.6	20.4
LR5	300x150x5	400	30	0.3	22.35
				0.45	20.435
				0.6	15.824

Figure 22 shows the effect of load ratio on FR time for different yield strengths of steel. It is obvious from Figure 22 that with the increase in load ratio, the FR time decreased. By increasing the load ratio from 0.3 to 0.45 and 0.6, the FR time of LR1 group was found to decrease by 9% and 18%, respectively. The percentage decrease was similar for different yield strengths of steel. This is due to the fact that, residual strength of the member is less at higher load ratios and vice versa. It is important to mention that during analysis it was observed that the decrease in FR time with increase in load ratio was less for smaller cross-sections as compared to larger cross-sections due to the lesser amount of steel area exposed to fire. Similar conclusions were made by researchers for concrete filled stainless steel tube (Han et al., 2013) and concrete filled double steel tube (Wan et al., 2017) subjected to axial load at elevated temperature.

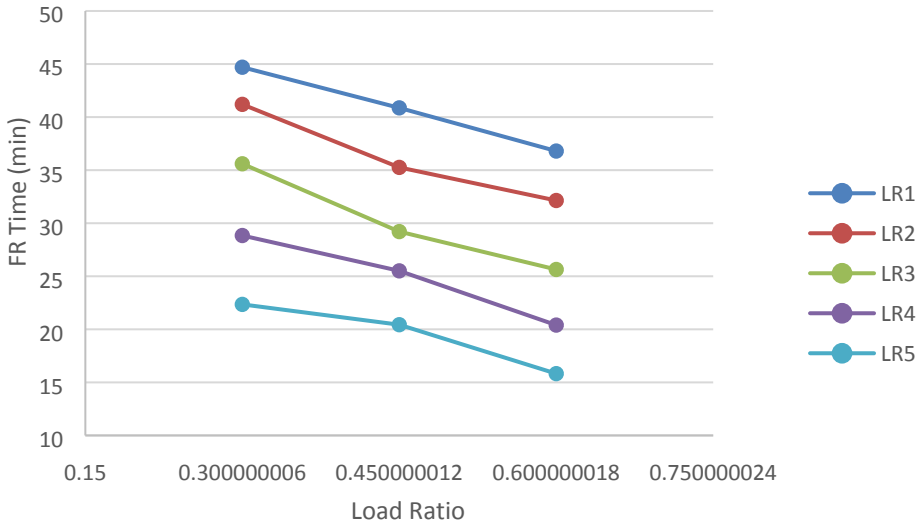

Figure 22 Effect of load ratio on FR time for different yield strengths of steel

5.4. Effect of width-to-depth ratio (B/D ratio)

The influence of B/D ratio on the FR time of CFST member subjected to flexural load is shown in Figure 23 and Table 11 respectively. For SR1 group, the FR time for cross-section having dimensions of 300 x 150 and 300 x 300 was 44.7 and 62.58 minutes respectively. This shows an increase of 40% FR time for 300 x 300over 300 x 150. In addition to higher FR time, the surface temperature of larger cross-sections will also rise slowly hence leading to slower reduction in flexural capacity. This is logical, since a CFST member with larger cross-section dimension has more infilled concrete, thus, the rise of temperature is slower in the inner part of the member, which increases its fire endurance.

Table 11 Details of models used to study the effect of B/D ratio and steel ratio

Group Name	DxBxt	fy	B/D ratio	fc	n	Steel ratio	FR Time
SR1	300x150x5	235	2	30	0.3	4.4%	44.7
	300x300x5		1			2.85%	62.58
	600x300x5		0.5			2.1%	91.6
SR2	300x150x5	275	2	30	0.3	4.4%	41.2
	300x300x5		1			2.85%	57.68
	600x300x5		0.5			2.1%	82.46
SR3	300x150x5	300	2	30	0.3	4.4%	35.6
	300x300x5		1			2.85%	49.84
	600x300x5		0.5			2.1%	73.51

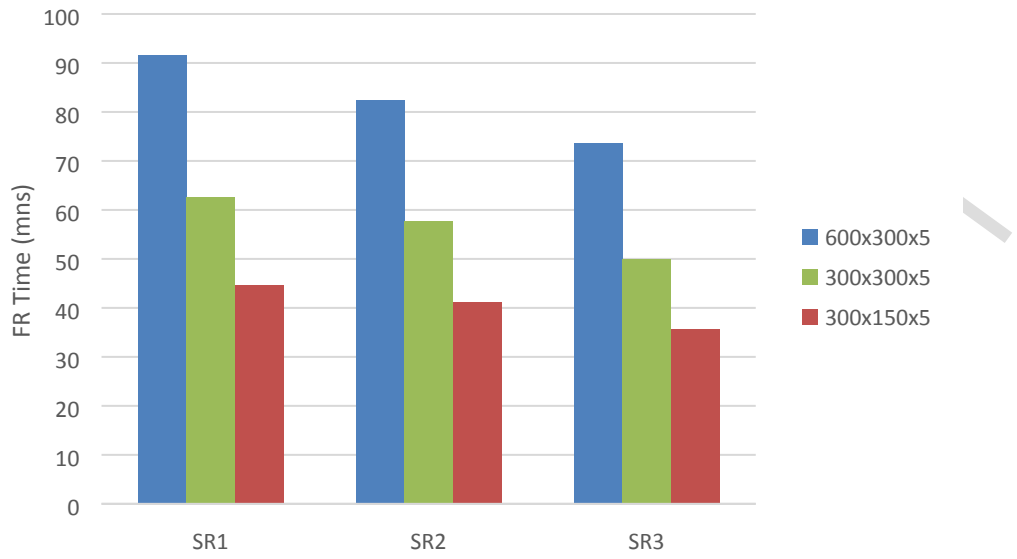

Figure 23 Comparison of FR time of different steel ratios and cross-sectional dimensions

5.5. Effect of steel ratio

Steel ratio is defined as the ratio of the area of steel to the area of concrete of CFST member. To study the effect of steel ratio on the FR time of CFST member, 3 cross-sectional dimensions were selected. The compressive strength of concrete is assumed to be 30 MPa. The detailed dimensions of the selected sections are shown in Table 11.

Figure 23 shows the effect of steel ratio on FR time of CFST member. It is obvious from Figure 23 that the FR time decrease D with the increase in steel ratio regardless of the yield strength of steel. When the steel ratio increased from 2.1% to 2.85% and 4.4%, the FR time of SR2 group was found to decrease by 31% and 51%, respectively. This is due to the usage of higher amount of steel. As the strength degradation of steel at elevated temperature is faster than concrete core, therefore CFST member with higher steel ratio attain its FR faster when subjected to elevated temperature (Han et al., 2013).

6. Comparison with previous data

6.1. Strength reduction factors

The comparison between moment reduction factors obtained from this experimental study with the moment reduction factors given by Chung et al. (2009) is shown in Figure 25. It can be seen that the predictions made by Chung et al. (2009) for flexural loads are accurate for the exposure time of 5 minutes. Thereafter, the difference between the predicted and experimental results increased and reached up to 20% at fire exposure time of 40 minutes. The strength reduction factors for square and rectangular members are similar with less than 5% of difference. Strength reduction factors of OCFST are higher than NCFST showing the better performance of OCFST at elevated

temperature. Furthermore, modification is recommended in the existing methods for calculating the strength reduction of members by considering the effect of flexural load and type of infilled concrete.

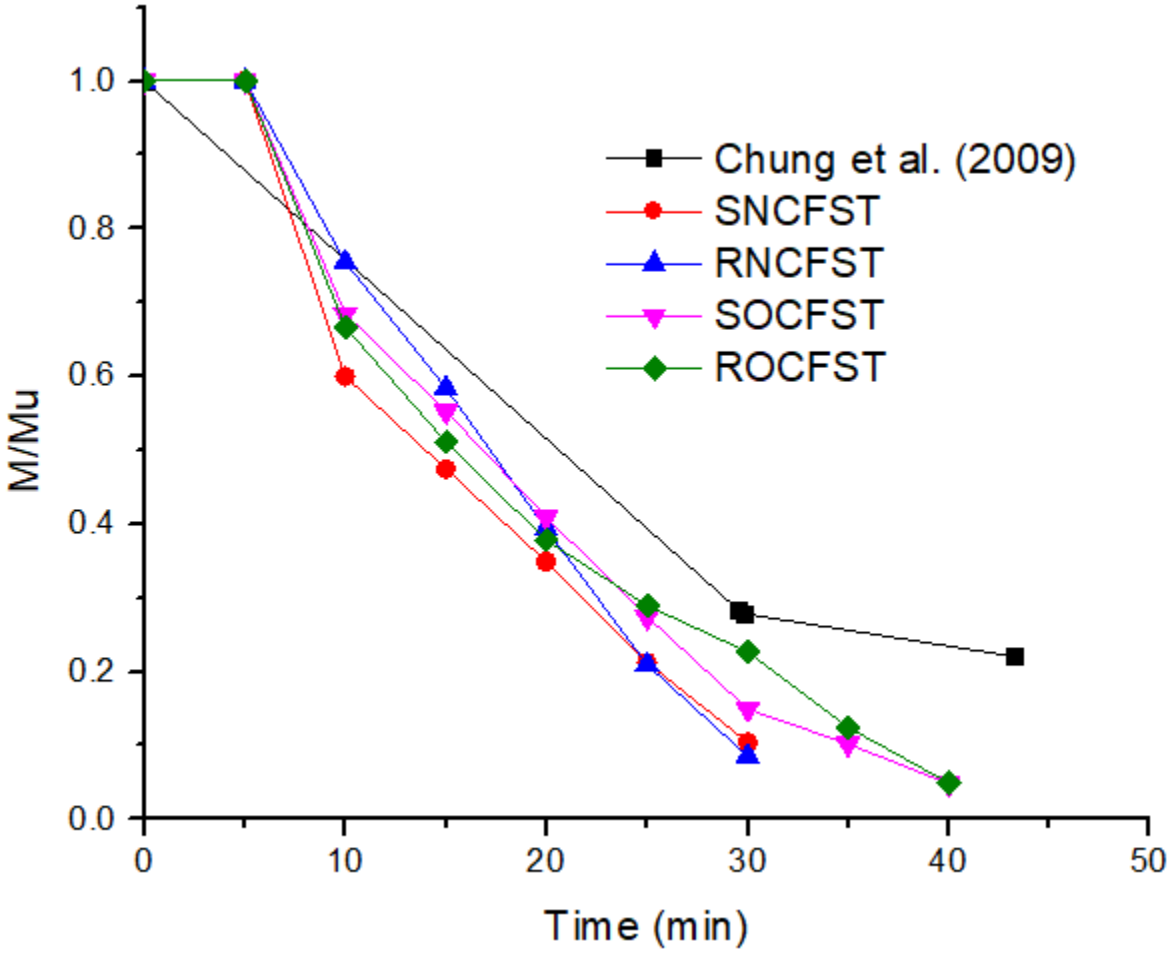

Figure 24 Comparison of moment reduction factors obtained from this experiment with results presented by Chung et al. (2009)

6.2. Temperature of Steel tube

As the specimen is exposed to elevated temperature, the temperature of the steel and infilled concrete rises with the passage of time. For CFST columns, different equations for predicting the temperature of steel tube at certain time are available in literature (Albero et al., 2016; Espinos et al., 2013; Ibañez et al., 2016; Wan et al., 2017; Yu et al., 2014) from which five different equations were selected to predict the temperature of the outer steel tube. The equations are published in (Albero et al., 2016; Espinos et al., 2013; Ibañez et al., 2016; Wan et al., 2017; Yu et al., 2014) and are given below.

$$T_s = -824.667 - 5.579R - 0.007R^2 - 0.009R\frac{A_m}{V} \mp 645.076(R)^{0.269}\left(\frac{A_m}{V}\right)^{0.017}$$ Equation (3) (Albero et al., 2016)

$$T_s = 342.1 + 10.77R - 0.044R^2 + \frac{3.922A_m}{V} - 0.025RA_m/V$$ Equation (4) (Espinos et al., 2013)

$$T_s = \phi_{room} + [345\log(8R+1)] * \left[1 - 3.38R^{-0.18}\right] * \left(1 - \left[0.155R^{0.58} + t^{-0.1}\right]\right)$$ Equation (5) (Ibañez et al., 2016)

$$T_s = 1200\left(1 - \frac{1}{1 + \left(\frac{R}{20.22 + 0.51t}\right)^{0.996 + 0.014t}}\right) + 20$$ Equation 5 (Wan et al., 2017)

$$T_s = 1200\left(1 - \frac{1}{1 + \left(\frac{R}{60(0.337 + 8.5d)}\right)^{0.996 + 14.0d}}\right) + 20$$ Equation (6) (Yu et al., 2014)

In the above equations, T_s is the temperature of steel tube, R is the fire exposure time in minutes, t is thickness of steel tube in mm, $\frac{A_m}{V}$ is section factor, and d is the equivalent thickness of steel in meters.

The predicted temperature using the above equations were compared with the average temperature (Sum of temperature of T1-T9 thermo-couples/9) obtained from the experiments performed. The comparison of temperature of steel tube obtained from the equations with experimental values is shown in Figure 26. Although, these equations were given for different cross-sections (ellipse, circular, square and rectangular) of CFST columns, yet they can be used for CFST beams having square and rectangular cross-sections. Equation 5 given in reference (Wan et al., 2017) yielded most accurate prediction because it took into account the average temperature of steel tube along its thickness and was based on both numerical and experimental results while equation 3 gave the least accurate results.

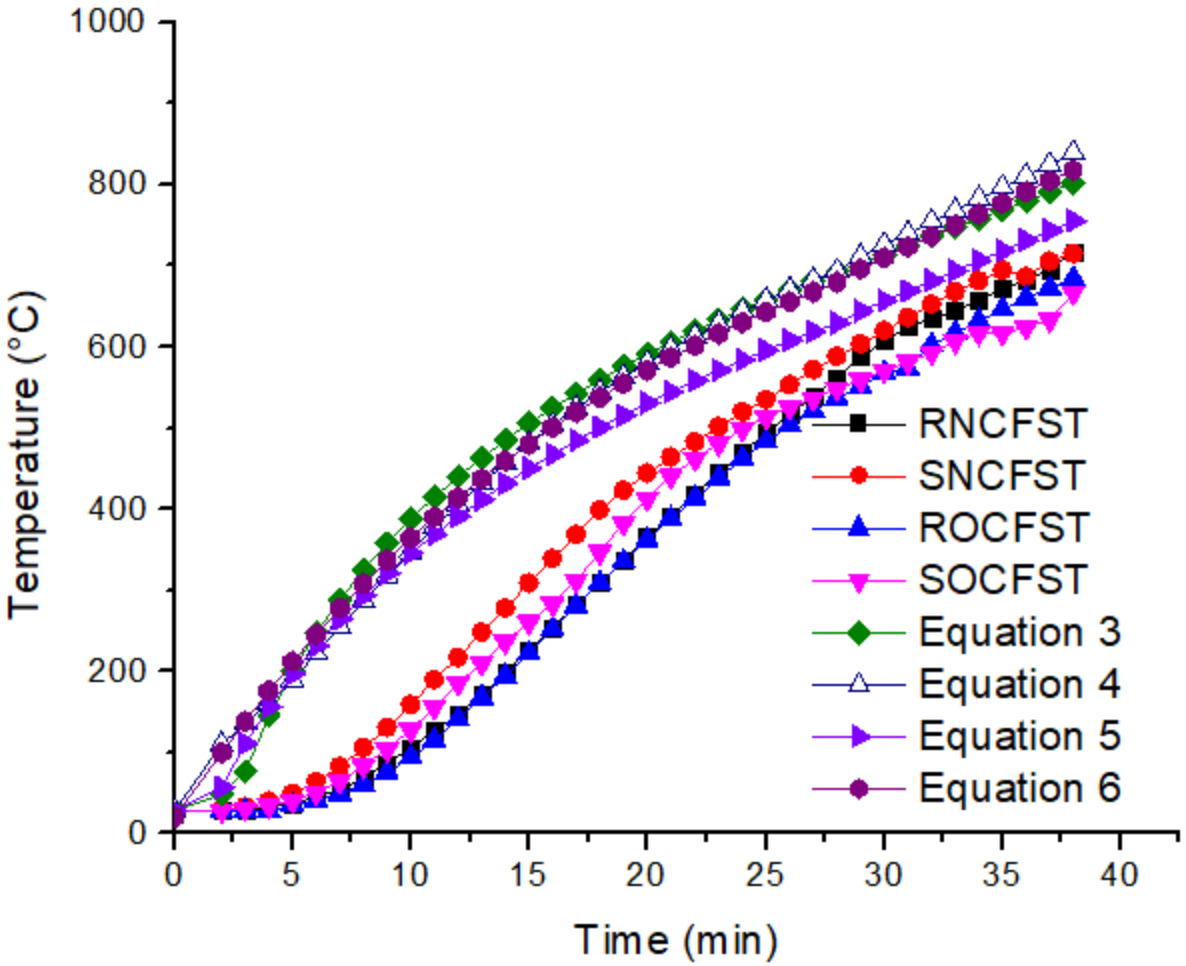

588

589 Figure 25 Comparison of temperature of outer steel of square CFST Beams with equations [3-6]

590 ### 6.3. Temperature of infilled concrete

591 The comparison of time-temperature curve of in-filled concrete calculated from the equations
592 recommended by different researchers for different shapes of CFST columns (Albero et al., 2016;
593 Espinos et al., 2013; Ibañez et al., 2016; Wan et al., 2017; Yu et al., 2014) and experimental results
594 from this research are shown in Figure 27. The predicted time-temperature curve obtained from
595 equation given by Espinos et al. (Espinos et al., 2013) has the difference of more than 15% when
596 compared with the experimental time-temperature curve throughout the fire exposure time. When
597 the time-temperature curve using equation given by Wan et al. (Wan et al., 2017) is compared with
598 experimental data, it can be seen that the experimental time-temperature curve followed closely at
599 the start of the test but lags by 100°C at the end of the test. The time-temperature values obtained
600 from equation given by Ibanez et al. (Ibañez et al., 2016) followed the experimental time-
601 temperature curve closely during the first 20 minutes but lagged at the end of the test. The lagging
602 is more prominent in square CFST as compared to rectangular CFST. Finally, the temperature
603 predicted by Albero et al. (Albero et al., 2016) is accurate till the end of the test for rectangular
604 CFST but lagged by more than 15% for square CFST. Hence, modification is recommended in the

existing equations by considering the effect of cross-section of steel tube, thickness of steel tube, type of infill concrete, type of steel and size of the furnace.

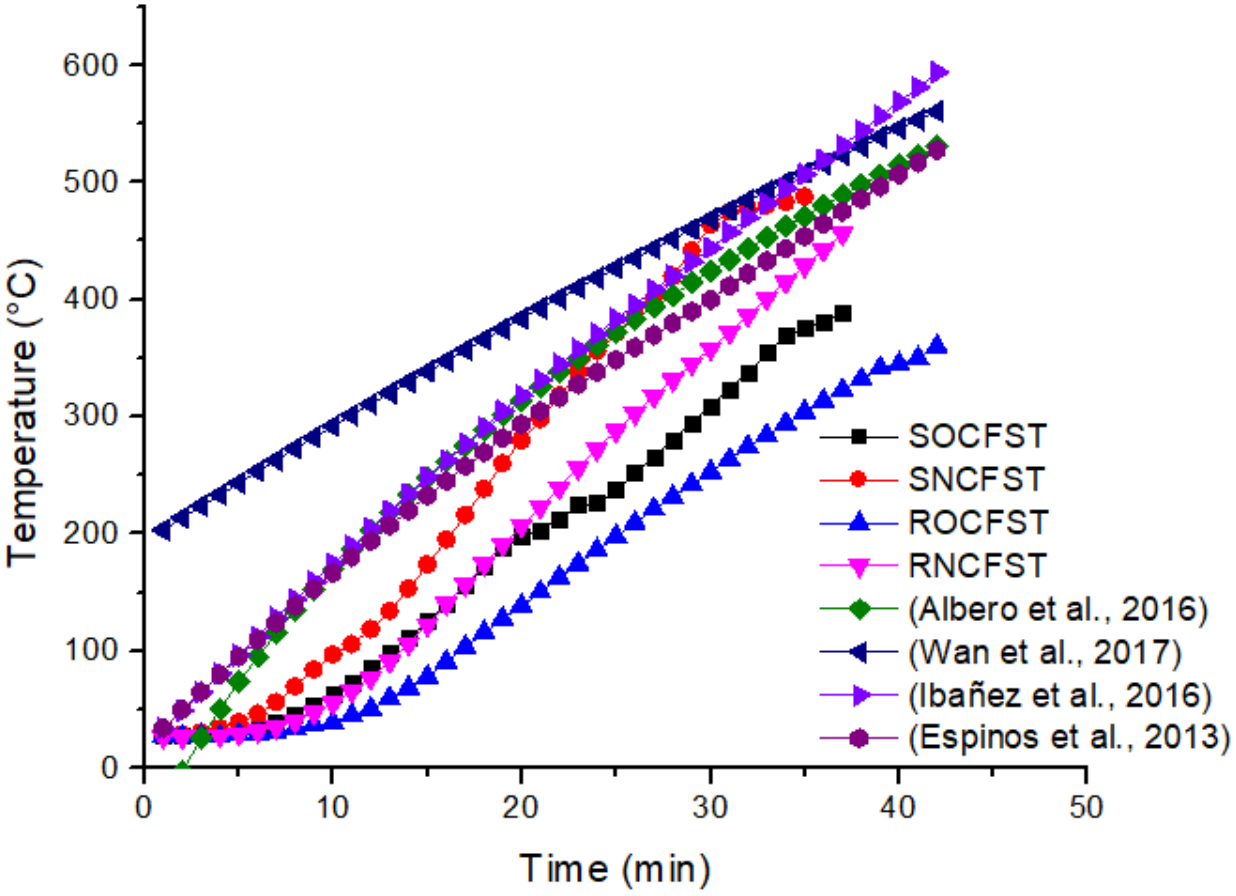

Figure 26 Comparison of temperature of infilled concrete of square CFST Beams with equations given in (Albero et al., 2016; Espinos et al., 2013; Ibañez et al., 2016; Wan et al., 2017)

7. Conclusions

The utilization of agricultural wastes in construction industry would be an ideal choice for sustainable and green construction. The oil palm industry produces a huge amount of solid agricultural wastes including oil palm boiler clinker (OPB). In this paper, a new sustainable and environment friendly composite flexural member with conventional coarse aggregate replaced with OPB was analyzed and its elevated temperature performance was compared with a conventional composite member. Based on experimental and numerical investigation, following conclusions can be drawn:

1. The deflection at any instant of time in OCFST was less than NCFST due to low temperature rise in steel tube and higher contribution of infilled concrete. Moreover, the

higher limiting values temperature in OCFST than NCFST reflects better fire resistance of OCFST beams.

2. The critical time of OCFST was 8-10 min higher than NCFST. Similarly, fire concrete contribution ratio of OCFST was found to be 30% higher than NCFST showing superior structural performance of OCFST at elevated temperature.
3. FE model was used to investigate the effect of yield strength of steel, compressive strength of infilled concrete, load ratio, width-to-depth ratio and steel ratio. It was found that by changing the yield strength of steel tube from 235 to 400 MPa, steel ratio from 2.1% to 4.4% and load ratio from 0.3 to 0.6, the fire resistance time of CFST members decreased from 44 to 22 min (50%), 91.6 to 44.4 min (51%) and 44 to 36 min (18%), respectively. However, FR time increased by 57% when the compressive strength of infilled concrete increased from 30 to 75 MPa.
4. The experimental results when compared with existing equations developed for CFST columns filled with natural aggregate concrete indicated that current equations may underestimate the fire resistance of CFST filled with OPB.

Conclusively, the OCFST beams can be introduced as a new sustainable and eco-friendly composite beam due to its better structural performance at elevated temperature.

References

Abid, M., Hou, X., Zheng, W., Hussain, R.R., 2017. High temperature and residual properties of reactive powder concrete–A review. Construction and Building Materials 147, 339-351.

ACI Committee 318, 2015. Building Code Requirements for Structural Concrete (ACI 318-14): An ACI Standard: Commentary on Building Code Requirements for Structural Concrete (ACI 318R-14), an ACI Report. American Concrete Institute.

Albero, V., Espinos, A., Romero, M.L., Hospitaler, A., Bihina, G., Renaud, C., 2016. Proposal of a new method in EN1994-1-2 for the fire design of concrete-filled steel tubular columns. Engineering Structures 128, 237-255.

Aslam, M., Shafigh, P., Jumaat, M.Z., 2016a. Drying shrinkage behaviour of structural lightweight aggregate concrete containing blended oil palm bio-products. Journal of cleaner production 127, 183-194.

Aslam, M., Shafigh, P., Jumaat, M.Z., 2016b. Oil-palm by-products as lightweight aggregate in concrete mixture: a review. Journal of Cleaner Production 126, 56-73.

Aslam, M., Shafigh, P., Jumaat, M.Z., 2017. High Strength Lightweight Aggregate Concrete using Blended Coarse Lightweight Aggregate Origin from Palm Oil Industry. Sains Malaysiana 46(4), 667-675.

Aslam, M., Shafigh, P., Jumaat, M.Z., Lachemi, M., 2016c. Benefits of using blended waste coarse lightweight aggregates in structural lightweight aggregate concrete. Journal of Cleaner Production 119, 108-117.

Bessou, C., Chase, L.D.C., Henson, I.E., Abdul-Manan, A.F.N., Milà i Canals, L., Agus, F., Sharma, M., Chin, M., 2014. Pilot application of PalmGHG, the Roundtable on Sustainable Palm Oil greenhouse gas calculator for oil palm products. Journal of Cleaner Production 73, 136-145.

CEN, E., 2006. 1-3, Eurocode 3–Design of steel structures–Part 1-3: General rules–Supplementary rules for coldformed members and sheeting. European Committee for Standardization, Bruxelles.

662 Chen, Z., Xu, J., Chen, Y., Lui, E.M., 2016. Recycling and reuse of construction and demolition waste in
663 concrete-filled steel tubes: A review. Construction and Building Materials 126, 641-660.
664 Chung, K., Park, S., Choi, S., 2009. Fire resistance of concrete filled square steel tube columns subjected
665 to eccentric axial load. International Journal of Steel Structures 9(1), 69-76.
666 Craveiro, H.D., Rodrigues, J.P.C., Laím, L., 2016. Experimental analysis of built-up closed cold-formed steel
667 columns with restrained thermal elongation under fire conditions. Thin-Walled Structures 107, 564-
668 579.
669 de Normalisation, C.E., 1994. Eurocode 4: Design of composite steel and concrete structures. part 1-2:
670 General rules-structural fire design. CEN ENV.
671 Ding, J., Wang, Y.C., 2008. Realistic modelling of thermal and structural behaviour of unprotected concrete
672 filled tubular columns in fire. Journal of Constructional Steel Research 64(10), 1086-1102.
673 Dong, C.X., Kwan, A.K.H., Ho, J.C.M., 2015. A constitutive model for predicting the lateral strain of confined
674 concrete. Engineering Structures 91, 155-166.
675 EN, B., 1991. 1-2: 2002 Eurocode 1: Actions on structures—Part 1-2: General actions—Actions on
676 structures exposed to fire. British Standards.
677 EN, B., 2004. 1-2: 2004 Eurocode 2: Design of concrete structures-Part 1-2: General rules-Structural fire
678 design. European Standards, London.
679 Espinos, A., 2012. Numerical analysis of the fire resistance of circular and elliptical slender concrete filled
680 tubular columns. Doctoral thesis. Valencia, Spain: Universitat Politècnica de València.
681 Espinos, A., Romero, M.L., Hospitaler, A., 2013. Fire design method for bar-reinforced circular and elliptical
682 concrete filled tubular columns. Engineering Structures 56, 384-395.
683 Franssen, J.-M., Real, P.V., 2016. Fire Design of Steel Structures: EC1: Actions on structures; Part 1-2:
684 Actions on structure exposed to fire; EC3: Design of steel structures; Part 1-2: Structural fire design.
685 John Wiley & Sons.
686 Fu, Z., Ji, B., Ge, H., Yang, M., 2015. Combined strength of lightweight aggregate concrete-filled steel tube.
687 Materials Research Innovations 19(sup5), S5-898-S895-901.
688 GB50936, 2014. Steel tube concrete structure technical specification [S].
689 Hamidian, M.R., Shafigh, P., Jumaat, M.Z., Alengaram, U.J., Sulong, N.R., 2016. A new sustainable
690 composite column using an agricultural solid waste as aggregate. Journal of Cleaner Production 129,
691 282-291.
692 Han, L.-H., Chen, F., Liao, F.-Y., Tao, Z., Uy, B., 2013. Fire performance of concrete filled stainless steel
693 tubular columns. Engineering Structures 56, 165-181.
694 Han, L.-h., Tao, Z., Liu, W., 2001. Concrete filled steel tubular structures from theory to practice [J]. Journal
695 of Fuzhou University (Natural Sciences Edtion) 6, 003.
696 Han, L.-H., Zhao, X.-L., Yang, Y.-F., Feng, J.-B., 2003. Experimental study and calculation of fire resistance
697 of concrete-filled hollow steel columns. Journal of structural engineering 129(3), 346-356.
698 Hartono, H., Chai, L.J., Lee, B., 2016. Lightweight Concrete Using Oil Palm Boiler Clinker (OPBC)-A Review,
699 MATEC Web of Conferences. EDP Sciences.
700 Hong, S., Varma, A.H., 2009. Analytical modeling of the standard fire behavior of loaded CFT columns.
701 Journal of Constructional Steel Research 65(1), 54-69.
702 Huo, J., Xiao, Y., Ren, X., Zeng, X., 2015. A new hybrid heating method used in fire test. Experimental
703 Thermal and Fluid Science 62, 52-57.
704 Ibañez, C., Romero, M.L., Hospitaler, A., 2016. Effects of axial and rotational restraints on concrete-filled
705 tubular columns under fire. Journal of Constructional Steel Research 125, 114-127.
706 Ibrahim, I., Hassan, M.A., Abd-Aziz, S., Shirai, Y., Andou, Y., Othman, M.R., Ali, A.A.M., Zakaria, M.R., 2017.
707 Reduction of residual pollutants from biologically treated palm oil mill effluent final discharge by
708 steam activated bioadsorbent from oil palm biomass. Journal of Cleaner Production 141, 122-127.

ISO 834:, 1999. Fire resistance tests-Elements of building construction. International Organization for Standardization, Geneva.

ISO 12570:, 2000. Hygrothermal performance of building materials and products -- Determination of moisture content by drying at elevated temperature. Comité Européen de Normalisation, Brussels, Belgium.

Javed, M., Ramli, N., Kashif-ur-Rehman, S., Khan, N., 2017. Finite element analysis on the structural behaviour of square CFST beams, IOP Conference Series: Materials Science and Engineering. IOP Publishing, p. 012018.

Javed, M.F., Hafizah, N., Memon, S.A., Jameel, M., Aslam, M., 2017a. Recent research on cold-formed steel beams and columns subjected to elevated temperature: A review. Construction and Building Materials 144, 686-701.

Javed, M.F., Sulong, N.R., Memon, S.A., Rehman, S.K.-U., Khan, N.B., 2018. Flexural behaviour of steel hollow sections filled with concrete that contains OPBC as coarse aggregate. Journal of Constructional Steel Research 148, 287-294.

Javed, M.F., Sulong, N.R., Memon, S.A., Rehman, S.K.U., Khan, N.B., 2017b. FE modelling of the flexural behaviour of square and rectangular steel tubes filled with normal and high strength concrete. Thin-Walled Structures 119, 470-481.

Jiang, A.-y., Chen, J., Jin, W.-l., 2013. Experimental investigation and design of thin-walled concrete-filled steel tubes subject to bending. Thin-Walled Structures 63, 44-50.

Jumaat, M.Z., Alengaram, U.J., Ahmmad, R., Bahri, S., Islam, A.S., 2015. Characteristics of palm oil clinker as replacement for oil palm shell in lightweight concrete subjected to elevated temperature. Construction and Building Materials 101, 942-951.

Kanadasan, J., Abdul Razak, H., 2015. Engineering and sustainability performance of self-compacting palm oil mill incinerated waste concrete. Journal of Cleaner Production 89, 78-86.

Kanadasan, J., Razak, H.A., 2015. Engineering and sustainability performance of self-compacting palm oil mill incinerated waste concrete. Journal of Cleaner Production 89, 78-86.

Karim, M.R., Islam, A., Chowdhury, F.I., Rehman, S.K.U., Islam, M.R., 2018. Ready mixed concrete behavior of granulated blast furnace slag contained cement. COMPUTERS AND CONCRETE 21(2), 139-147.

Kashif Ur Rehman, S., Ibrahim, Z., Memon, S.A., Aunkor, M.T.H., Faisal Javed, M., Mehmood, K., Shah, S.M.A., 2018. Influence of Graphene Nanosheets on Rheology, Microstructure, Strength Development and Self-Sensing Properties of Cement Based Composites. Sustainability 10(3), 822.

Kesawan, S., Mahendran, M., 2018. Post-fire mechanical properties of cold-formed steel hollow sections. Construction and Building Materials 161, 26-36.

Khan, N.B., Ibrahim, Z., Bin Mohamad Badry, A.B., Jameel, M., Javed, M.F., 2018. Numerical investigation of flow around cylinder at Reynolds number= 3900 with large eddy simulation technique: Effect of spanwise length and mesh resolution. Proceedings of the Institution of Mechanical Engineers, Part M: Journal of Engineering for the Maritime Environment, 1475090217751326.

Khan, N.B., Ibrahim, Z., Javed, M.F., Jameel, M., 2017. Numerical investigation of the vortex-induced vibration of an elastically mounted circular cylinder at high Reynolds number (Re= 104) and low mass ratio using the RANS code. PloS one 12(10), e0185832.

Kwan, A.K.H., Dong, C.X., Ho, J.C.M., 2015. Axial and lateral stress–strain model for FRP confined concrete. Engineering Structures 99, 285-295.

Laím, L., Rodrigues, J.P.C., Craveiro, H.D., 2016. Flexural behaviour of axially and rotationally restrained cold-formed steel beams subjected to fire. Thin-Walled Structures 98, Part A, 39-47.

Li, H.-T., Young, B., 2017. Material properties of cold-formed high strength steel at elevated temperatures. Thin-Walled Structures 115, 289-299.

Li, W., Luo, Z., Tao, Z., Duan, W.H., Shah, S.P., 2017. Mechanical behavior of recycled aggregate concrete-filled steel tube stub columns after exposure to elevated temperatures. Construction and Building Materials 146, 571-581.

Liu, J.-Q., Han, L.-H., Zhao, X.-L., 2018. Performance of concrete-filled steel tubular column-wall structure subjected to ISO-834 standard fire: analytical behaviour. Thin-Walled Structures 129, 28-44.

LRFD, A., 1994. Manual of steel construction, load and resistance factor design. Chicago: American Institute of Steel Construction.

Lu, H., Zhao, X.-L., Han, L.-H., 2009. Fire behaviour of high strength self-consolidating concrete filled steel tubular stub columns. Journal of constructional steel research 65(10), 1995-2010.

Malaysia, A.I., 2011. National Biomass Strategy 2020: New wealth creation for Malaysia's palm oil industry. Agensi Inovasi Malaysia.

Mo, K.H., Alengaram, U.J., Jumaat, M.Z., Liu, M.Y.J., Lim, J., 2016. Assessing some durability properties of sustainable lightweight oil palm shell concrete incorporating slag and manufactured sand. Journal of Cleaner Production 112, 763-770.

Mohammadhosseini, H., Yatim, J.M., 2017. Microstructure and residual properties of green concrete composites incorporating waste carpet fibers and palm oil fuel ash at elevated temperatures. Journal of Cleaner Production 144, 8-21.

Moliner, V., Espinos, A., Romero, M., Hospitaler, A., 2013. Fire behavior of eccentrically loaded slender high strength concrete-filled tubular columns. Journal of Constructional Steel Research 83, 137-146.

Musikavong, C., Gheewala, S.H., 2017a. Assessing ecological footprints of products from the rubber industry and palm oil mills in Thailand. Journal of Cleaner Production 142, 1148-1157.

Musikavong, C., Gheewala, S.H., 2017b. Ecological footprint assessment towards eco-efficient oil palm and rubber plantations in Thailand. Journal of Cleaner Production 140, 581-589.

Mustapa, S., Sulong, N., 2017. Performance of Palm Oil Clinker as a Bio-Filler with Hybrid Fillers in Intumescent Fire Protective Coatings for Steel. Sains Malaysiana 46(12), 2489-2496.

Nayaka, R.R., Alengaram, U.J., Jumaat, M.Z., Yusoff, S.B., Alnahhal, M.F., 2018. High volume cement replacement by environmental friendly industrial by-product palm oil clinker powder in cement–lime masonry mortar. Journal of Cleaner Production.

Ng, W.P.Q., Lam, H.L., Ng, F.Y., Kamal, M., Lim, J.H.E., 2012. Waste-to-wealth: green potential from palm biomass in Malaysia. Journal of Cleaner Production 34, 57-65.

Rehman, S.K.U., Ibrahim, Z., Memon, S.A., Jameel, M., 2016. Nondestructive test methods for concrete bridges: A review. Construction and Building Materials 107, 58-86.

Rehman, S.K.U., Ibrahim, Z., Memon, S.A., Javed, M.F., Khushnood, R.A., 2017. A sustainable graphene based cement composite. Sustainability 9(7), 1229.

Rodrigues, J.P.C., Laim, L., 2017. Fire response of restrained composite columns made with concrete filled hollow sections under different end-support conditions. Engineering Structures 141, 83-96.

Rodrigues, J.P.C., Laím, L., 2017. Fire resistance of restrained composite columns made of concrete filled hollow sections. Journal of Constructional Steel Research 133, 65-76.

Romero, M.L., Moliner, V., Espinos, A., Ibañez, C., Hospitaler, A., 2011. Fire behavior of axially loaded slender high strength concrete-filled tubular columns. Journal of Constructional Steel Research 67(12), 1953-1965.

Rush, D., Bisby, L., Melandinos, A., Lane, B., 2011. Fire resistance design of unprotected concrete filled steel hollow sections: meta-analysis of available furnace test data. Fire Safety Science 10, 1549-1562.

Saswattecha, K., Kroeze, C., Jawjit, W., Hein, L., 2015. Assessing the environmental impact of palm oil produced in Thailand. Journal of Cleaner Production 100, 150-169.

Sauca, A., Gernay, T., Robert, F., Tondini, N., Franssen, J.-M., 2016. Stability in hybrid fire testing, Proceedings of the 9th International Conference on Structures in Fire.

803 Shafigh, P., Mahmud, H.B., Jumaat, M.Z.B., Ahmmad, R., Bahri, S., 2014. Structural lightweight aggregate
804 concrete using two types of waste from the palm oil industry as aggregate. Journal of cleaner
805 production 80, 187-196.
806 Silva, A., Jiang, Y., Castro, J., Silvestre, N., Monteiro, R., 2016. Experimental assessment of the flexural
807 behaviour of circular rubberized concrete-filled steel tubes. Journal of Constructional Steel
808 Research 122, 557-570.
809 Suttayakul, P., H-Kittikun, A., Suksaroj, C., Mungkalasiri, J., Wisansuwannakorn, R., Musikavong, C., 2016.
810 Water footprints of products of oil palm plantations and palm oil mills in Thailand. Science of The
811 Total Environment 542, 521-529.
812 Tao, Z., Uy, B., Han, L.-H., Wang, Z.-B., 2009. Analysis and design of concrete-filled stiffened thin-walled
813 steel tubular columns under axial compression. Thin-Walled Structures 47(12), 1544-1556.
814 Teo, D., Mannan, M.A., Kurian, V., Ganapathy, C., 2007. Lightweight concrete made from oil palm shell
815 (OPS): structural bond and durability properties. Building and Environment 42(7), 2614-2621.
816 Tubes, B.S., Pipes.(1990).". Design for SHS fire resistance to BS5950: Part 8.
817 Ukanwa, K.U., Clifton, G.C., Lim, J.B., Hicks, S.J., Sharma, U., Abu, A., 2018. Simple design procedure for
818 concrete filled steel tubular columns in fire. Engineering Structures 155, 144-156.
819 Ukanwa, K.U., Sharma, U., Hicks, S.J., Abu, A., Lim, J.B., Clifton, G.C., 2017. Behaviour of continuous
820 concrete filled steel tubular columns loaded concentrically in fire. Journal of Constructional Steel
821 Research 136, 101-109.
822 Wan, C.-Y., Zha, X.-X., Dassekpo, J.-B.M., 2017. Analysis of axially loaded concrete filled circular hollow
823 double steel tubular columns exposed to fire. Fire Safety Journal 88, 1-12.
824 Wang, D., Wang, Z., Smith, S.T., Yu, T., 2016. Size effect on axial stress-strain behavior of CFRP-confined
825 square concrete columns. Construction and Building Materials 118, 116-126.
826 Wang, K., Young, B., 2013. Fire resistance of concrete-filled high strength steel tubular columns. Thin-
827 Walled Structures 71, 46-56.
828 Wang, Y., Kodur, V., 2000. Research toward use of unprotected steel structures. Journal of structural
829 engineering 126(12), 1442-1450.
830 Wang, Y.C., 2014. Steel and composite structures: Behaviour and design for fire safety. CRC Press.
831 Yang, H., Liu, F., Zhang, S., Lv, X., 2013. Experimental investigation of concrete-filled square hollow section
832 columns subjected to non-uniform exposure. Engineering Structures 48, 292-312.
833 Yang, Y.-F., Han, L.-H., 2006. Experimental behaviour of recycled aggregate concrete filled steel tubular
834 columns. Journal of Constructional Steel Research 62(12), 1310-1324.
835 Yu, M., Pei, X., Xu, L., Ye, J., 2018. A unified formula for calculating bending capacity of solid and hollow
836 concrete-filled steel tubes under normal and elevated temperature. Journal of Constructional Steel
837 Research 141, 216-225.
838 Yu, M., Zha, X., Ye, J., Wang, B., 2014. A unified method for calculating fire resistance of solid and hollow
839 concrete-filled steel tube columns based on average temperature. Engineering Structures 71, 12-
840 22.

841

Highlights

This paper presents a novel composite beam by using OPBC as coarse aggregate.

FE model was used to evaluate the effect of different parameters in fire.

The deflection in OCFST was less than NCFST due to low temperature rise in steel.

OCFST has 30% higher FR time and fire concrete contribution ratio than NCFST.